Computational Mechanics (2022) 69:1069–1086
https://doi.org/10.1007/s00466-021-02121-2

ORIGINAL PAPER

Monotonicity-based regularization for shape reconstruction in linear elasticity

Sarah Eberle[1] · **Bastian Harrach**[1]

Received: 4 June 2021 / Accepted: 4 November 2021 / Published online: 11 March 2022

Abstract
We deal with the shape reconstruction of inclusions in elastic bodies. For solving this inverse problem in practice, data fitting functionals are used. Those work better than the rigorous monotonicity methods from Eberle and Harrach (Inverse Probl 37(4):045006, 2021), but have no rigorously proven convergence theory. Therefore we show how the monotonicity methods can be converted into a regularization method for a data-fitting functional without losing the convergence properties of the monotonicity methods. This is a great advantage and a significant improvement over standard regularization techniques. In more detail, we introduce constraints on the minimization problem of the residual based on the monotonicity methods and prove the existence and uniqueness of a minimizer as well as the convergence of the method for noisy data. In addition, we compare numerical reconstructions of inclusions based on the monotonicity-based regularization with a standard approach (one-step linearization with Tikhonov-like regularization), which also shows the robustness of our method regarding noise in practice.

Keywords Linear elasticity · Inverse problem · Shape reconstruction · One-step linearization method · Monotonicity-based regularization

Mathematics Subject Classification 35R30 · 65M32

1 Introduction

The main motivation is the non-destructive testing of elastic structures, such as is required for material examinations, in exploration geophysics, and for medical diagnostics (elastography). From a mathematical point of view, this constitutes an inverse problem since we have only measurement data on the boundary and not inside of the elastic body. This problem is highly ill-posed, since even the smallest measurement errors can completely falsify the result.

There are several authors who deal with the theory of the inverse problem of elasticity. For the two dimensional case, we refer the reader to [14,15,17,21]. In three dimensions, Nakamura and Uhlmann [22,23] and Eskin and Ralston [8] gave the proof for uniqueness results for both Lamé coefficients under the assumption that μ is close to a positive constant. Beretta et al. [2,3] proved the uniqueness for partial data, where the Lamé parameters are piecewise constant and some boundary determination results were shown in [17,20,22].

Further on, solution methods applied so far for the inverse problem, which will be solved in this paper, were presented in the following works: In Oberai et al. [24,25], the time-independent inverse problem of linear elasticity is solved by means of the adjoint method and the reconstruction is simulated numerically. In addition, Seidl et al. [26] deals with the coupling of the state and adjoint equation and added two variants of residual-based stabilization to solve the inverse linear elasticity problem for incompressible plane stress. A boundary element-Landweber method for the Cauchy problem in stationary linear elasticity was investigated in Marin and Lesnic [19]. In Hubmer et al. [13], the stationary inverse problem was solved by means of a Landweber iteration as well and numerical examples were presented. Reciprocity principles for the detection of cracks in elastic bodies were

✉ Sarah Eberle
eberle@math.uni-frankfurt.de

Bastian Harrach
harrach@math.uni-frankfurt.de

[1] Institute of Mathematics, Goethe-University Frankfurt, Frankfurt am Main, Germany

investigated, for example, in Andrieux et al. [1] and Steinhorst and Sändig [27] or more recently in Ferrier et al. [9]. By means of a regularization approach, a stationary elastic inverse problem is solved in Jadamba et al. [16] and applied in numerical examples. Marin and Lesnic [18] introduces a regularized boundary element method. Finally, we want to mention the monotonicity methods for linear elasticity developed by the authors of this paper in Eberle and Harrach [5] as well as its application for the reconstruction of inclusions based on experimental data in Eberle and Moll [7].

We want to point out that the reconstruction of the support of the Lamé parameters, also called shape in this paper, and not the reconstruction of their values is the topic of this work. The key issue of the shape reconstruction of inclusions is the monotonicity property of the corresponding Neumann-to-Dirichlet operator (see [28,29]). These monotonicity properties were also applied for the construction of monotonicity tests for electrical impedance tomography (EIT), e.g., in [12], as well as the monotonicity-based regularization in Harrach and Mach [11]. In practice however, data fitting functionals provide better results than the monotonicity methods but the data-fitting functionals are usually not convex (see, e.g. [10]). Even for exact data, therefore, it cannot generally be guaranteed that the algorithm does not erroneously deliver a local minimum. In addition, there is noise and ill-posedness. The local convergence theory of Newton-like methods requires non-linearity assumptions such as the tangential cone condition, which are still not proven even for simpler examples such as EIT. The convergence theory of Tikhonov-regularized data fitting functionals applies to their global minima, which in general cannot be found due to the non-convexity. Our method is based on the minimization of a convex functional and is to the knowledge of the authors the first rigorously convergent method for this problem, but only provides the shape of the inclusions. We combine the monotonicity methods (cf. [5,6]) with data fitting functionals to obtain convergence results and an improvement of both methods regarding stability for noisy data. Here, we want to remark that compared to other data-fitting methods, we use the following a-priori assumptions: the Lamé parameters fulfill monotonicity relations, have a common support, the lower and upper bounds of the contrasts of the anomalies are known and we deal with a constant and known background material. Compared with Harrach and Mach [11], we expand the approach used there from the consideration of only one parameter to two parameters.

The outline of the paper is as follows: We start with the introduction of the problem statement. In order to detect and reconstruct inclusions in elastic bodies, we aim to determine the difference between an unknown Lamé parameter pair (λ, μ) and that of the known background (λ_0, μ_0) and formulate a minimization problem. Similar to the linearized monotonicity tests in Eberle and Harrach [5], we also consider the Fréchet derivative, which approximates the difference between two Neumann-to-Dirichlet operators. For solving the resulting minimization problem, we first take a look at a standard approach (standard one-step linearization method). Therefore regularization parameters are introduced, which can only be determined heuristically. For this purpose, for example, a parameter study can be carried out. We would like to point out that this method is only a heuristic approach, but is commonly used in practice. Overall, this heuristic approach leads to reconstructions of the unknown inclusions without a rigorous theory. In Sect. 4, we focus on the monotonicity-based regularization in order to enhance the data fitting functionals. The idea of the regularization is to introduce conditions for the parameters / inclusions to be reconstructed for the minimization problem, which are based on the monotonicity properties of the Neumann-to-Dirichlet operator and the monotonicity tests. Further on, we prove that there exists a unique minimizer for this problem and that we obtain convergence even for noisy data. Finally, we compare numerical reconstructions of inclusions based on the monotonicity-based regularization with the one-step linearization, which also shows the robustness of our method regarding noise in practice.

2 Problem statement

We start with the introduction of the problems of interest, e.g., the *direct* as well as *inverse problem* of stationary linear elasticity.

Let $\Omega \subset \mathbb{R}^d$ ($d = 2$ or 3) be a bounded and connected open set with Lipschitz boundary $\partial\Omega = \Gamma = \overline{\Gamma_D \cup \Gamma_N}$, $\Gamma_D \cap \Gamma_N = \emptyset$, where Γ_D and Γ_N are the corresponding Dirichlet and Neumann boundaries. We assume that Γ_D and Γ_N are relatively open and connected. For the following, we define

$$L^\infty_+(\Omega) := \{w \in L^\infty(\Omega) : \operatorname*{ess\,inf}_{x\in\Omega} w(x) > 0\}.$$

Let $u : \Omega \to \mathbb{R}^d$ be the displacement vector, $\mu, \lambda : \Omega \to L^\infty_+(\Omega)$ the Lamé parameters, $\hat{\nabla} u = \frac{1}{2}\left(\nabla u + (\nabla u)^T\right)$ the symmetric gradient, n is the normal vector pointing outside of Ω , $g \in L^2(\Gamma_N)^d$ the boundary force and I the $d \times d$-identity matrix. We define the divergence of a matrix $A \in \mathbb{R}^{d\times d}$ via $\nabla \cdot A = \sum_{i,j=1}^{d} \frac{\partial A_{ij}}{\partial x_j} e_i$, where e_i is a unit vector and x_j a component of a vector from $\mathbb{R}^d$.

The boundary value problem of linear elasticity (*direct problem*) is that $u \in H^1(\Omega)^d$ solves

$$\nabla \cdot \left(\lambda(\nabla \cdot u)I + 2\mu\hat{\nabla} u\right) = 0 \quad \text{in } \Omega, \tag{1}$$

$$\left(\lambda(\nabla \cdot u)I + 2\mu\hat{\nabla}u\right) n = g \quad \text{on } \Gamma_N, \tag{2}$$

$$u = 0 \quad \text{on } \Gamma_D. \tag{3}$$

From a physical point of view, this means that we deal with an elastic test body Ω which is fixed (zero displacement) at Γ_D (Dirichlet condition) and apply a force g on Γ_N (Neumann condition). This results in the displacement u, which is measured on the boundary Γ_N.

The equivalent weak formulation of the boundary value problem (1)–(3) is that $u \in \mathcal{V}$ fulfills

$$\int_\Omega 2\mu\, \hat{\nabla}u : \hat{\nabla}v + \lambda \nabla \cdot u\, \nabla \cdot v\, dx = \int_{\Gamma_N} g \cdot v\, ds \quad \text{for all } v \in \mathcal{V}, \tag{4}$$

where $\mathcal{V} := \left\{ v \in H^1(\Omega)^d : v_{|\Gamma_D} = 0 \right\}$.

We want to remark that for $\lambda, \mu \in L^\infty_+(\Omega)$ the existence and uniqueness of a solution to the variational formulation (4) can be shown by the Lax-Milgram theorem (see e.g., in [4]).

Measuring boundary displacements that result from applying forces to Γ_N can be modeled by the Neumann-to-Dirichlet operator $\Lambda(\lambda, \mu)$ defined by

$$\Lambda(\lambda, \mu) : L^2(\Gamma_N)^d \to L^2(\Gamma_N)^d : \quad g \mapsto u_{|\Gamma_N},$$

where $u \in \mathcal{V}$ solves (1)–(3).

This operator is self-adjoint, compact and linear (see Corollary 1.1 from [5]). Its associated bilinear form is given by

$$\langle g, \Lambda(\lambda, \mu)h\rangle = \int_\Omega 2\mu\, \hat{\nabla}u^g_{(\lambda,\mu)} : \hat{\nabla}u^h_{(\lambda,\mu)} + \lambda \nabla \cdot u^g_{(\lambda,\mu)}\, \nabla \cdot u^h_{(\lambda,\mu)}\, dx, \tag{5}$$

where $u^g_{(\lambda,\mu)}$ solves the problem (1)–(3) and $u^h_{(\lambda,\mu)}$ the corresponding problem with boundary force $h \in L^2(\Gamma_N)^d$.

Another important property of $\Lambda(\lambda, \mu)$ is its Fréchet differentiability (for the corresponding proof see Lemma 2.3 in [5]). For directions $\hat{\lambda}, \hat{\mu} \in L^\infty(\Omega)$, the derivative

$$\Lambda'(\lambda, \mu)(\hat{\lambda}, \hat{\mu}) : L^2(\Gamma_N)^d \to L^2(\Gamma_N)^d$$

is the self-adjoint compact linear operator associated to the bilinear form

$$\langle \Lambda'(\lambda, \mu)(\hat{\lambda}, \hat{\mu})g, h\rangle = -\int_\Omega 2\hat{\mu}\, \hat{\nabla}u^g_{(\lambda,\mu)} : \hat{\nabla}u^h_{(\lambda,\mu)} + \hat{\lambda} \nabla \cdot u^g_{(\lambda,\mu)}\, \nabla \cdot u^h_{(\lambda,\mu)}\, dx.$$

Note that for $\hat{\lambda}_0, \hat{\lambda}_1, \hat{\mu}_0, \hat{\mu}_1 \in L^\infty(\Omega)$ with $\hat{\lambda}_0 \le \hat{\lambda}_1$ and $\hat{\mu}_0 \le \hat{\mu}_1$ we obviously have

$$\Lambda'(\lambda, \mu)(\hat{\lambda}_0, \hat{\mu}_0) \ge \Lambda'(\lambda, \mu)(\hat{\lambda}_1, \hat{\mu}_1), \tag{6}$$

in the sense of quadratic forms.

The *inverse problem* we consider here is the following

Find the support of $(\lambda - \lambda_0, \mu - \mu_0)^T$ *knowing the Neumann − to − Dirichlet operator* $\Lambda(\lambda, \mu)$.

Next, we take a look at the discrete setting. Let the Neumann boundary Γ_N be the union of the patches $\Gamma_N^{(l)}, l = 1, \ldots, M$, which are assumed to be relatively open and connected, such that $\overline{\Gamma_N} = \bigcup_{l=1}^M \overline{\Gamma_N^{(l)}}$, $\Gamma_N^{(i)} \cap \Gamma_N^{(j)} = \emptyset$ for $i \neq j$ and we consider the following problem:

$$\nabla \cdot \left(\lambda(\nabla \cdot u)I + 2\mu\hat{\nabla}u\right) = 0 \quad \text{in } \Omega, \tag{7}$$

$$\left(\lambda(\nabla \cdot u)I + 2\mu\hat{\nabla}u\right) n = g_l \quad \text{on } \Gamma_N^{(l)}, \tag{8}$$

$$\left(\lambda(\nabla \cdot u)I + 2\mu\hat{\nabla}u\right) n = 0 \quad \text{on } \Gamma_N^{(i)}, \quad i \neq l, \tag{9}$$

$$u = 0 \quad \text{on } \Gamma_D, \tag{10}$$

where g_l, $l = 1, \ldots, M$, denote the M given boundary forces applied to the corresponding patches $\Gamma_N^{(l)}$. In order to discretize the Neumann-to-Dirichlet operator, we apply a boundary force g_l on the patch $\Gamma_N^{(l)}$ and set

$$\Lambda_l^{(k)}(\lambda, \mu) := \int_{\Gamma_N^{(l)}} g_l \cdot u^{(k)}\, ds$$

(cf. (4) and (5)), where $u^{(k)}$ solves the corresponding boundary value problem (7)–(10) with boundary force g_k.

In Fig. 1 a simple example of possible boundary loads g_l and patches $\Gamma_N^{(l)}$ is shown.

For the Neumann boundary forces as described here, we get an orthogonal system g_l in $L^2(\Gamma_N)^d$. In practice, we additionally normalize the system g_l and use more patches $\Gamma_N^{(l)}$.

For the unknown Lamé parameters (λ, μ), we obtain a full matrix

$$\mathbf{\Lambda}(\lambda, \mu) = \left(\Lambda_l^{(k)}(\lambda, \mu)\right)_{k,l=1,\ldots,M}.$$

3 Standard one-step linearization methods

In this section we take a look at one-step linearization methods. We want to remark that these methods are only a heuristical approach but commonly used in practice.

We compare the matrix of the discretized Neumann-to-Dirichlet operator $\mathbf{\Lambda}(\lambda, \mu)$ with $\mathbf{\Lambda}(\lambda_0, \mu_0)$ for some reference Lamé parameter (λ_0, μ_0) in order to reconstruct

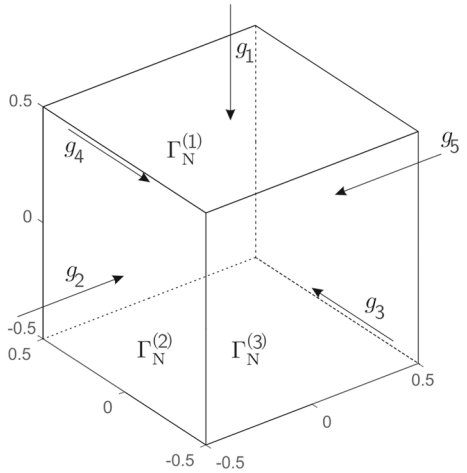

Fig. 1 Illustration of possible boundary loads g_l and patches $\Gamma_N^{(l)}$. We consider here $l = 1, \ldots, 5$, Neumann patches and one Dirichlet patch (bottom of the cube). The boundary forces g_l are normal vectors from the Euclidean space in each point of the patch

the difference $(\lambda, \mu) - (\lambda_0, \mu_0)$. Thus, we apply a single linearization step

$$\boldsymbol{\Lambda}'(\lambda_0, \mu_0)\left((\lambda, \mu) - (\lambda_0, \mu_0)\right) \approx \boldsymbol{\Lambda}(\lambda, \mu) - \boldsymbol{\Lambda}(\lambda_0, \mu_0),$$

where

$$\boldsymbol{\Lambda}'(\lambda_0, \mu_0) : L^\infty(\Omega)^2 \to \mathbb{R}^{M \times M}$$

is the Fréchet derivative which maps $(\hat{\lambda}, \hat{\mu}) \in L^\infty(\Omega)^2$ to

$$-\left(\int_\Omega \hat{\lambda}\left(\nabla \cdot u^{(k)}_{(\lambda_0,\mu_0)}\right)\left(\nabla \cdot u^{(l)}_{(\lambda_0,\mu_0)}\right) + 2\hat{\mu}\left(\hat{\nabla} u^{(k)}_{(\lambda_0,\mu_0)}\right) : \left(\hat{\nabla} u^{(l)}_{(\lambda_0,\mu_0)}\right) dx\right)_{1 \le k,l \le M}.$$

For the solution of the problem, we discretize the reference domain $\overline{\Omega} = \bigcup_{j=1}^p \overline{\mathcal{B}}_j$ into p disjoint pixel $\mathcal{B}_j$, where each $\mathcal{B}_j$ is assumed to be open, $\Omega \backslash \mathcal{B}_j$ is connected and $\mathcal{B}_j \cap \mathcal{B}_i = \emptyset$ for $j \neq i$. We make a piecewise constant ansatz for $(\kappa, \nu) \approx (\lambda, \mu) - (\lambda_0, \mu_0)$ via

$$\kappa(x) = \sum_{j=1}^p \kappa_j \chi_{\mathcal{B}_j}(x) \quad \text{and} \quad \nu(x) = \sum_{j=1}^p \nu_j \chi_{\mathcal{B}_j}(x), \tag{11}$$

where $\chi_{\mathcal{B}_j}$ is the characteristic function w.r.t. the pixel $\mathcal{B}_j$ and set

$$\boldsymbol{\kappa} = (\kappa_j)_{j=1}^p \in \mathbb{R}^p \quad \text{and} \quad \boldsymbol{\nu} = (\nu_j)_{j=1}^p \in \mathbb{R}^p.$$

This approach leads to the linear equation system

$$\mathbf{S}^\lambda \boldsymbol{\kappa} + \mathbf{S}^\mu \boldsymbol{\nu} = \mathbf{V}, \tag{12}$$

where $\mathbf{V}$ and the columns of the sensitivity matrices $\boldsymbol{S}^\lambda$ and $\boldsymbol{S}^\mu$ contain the entries of $\Lambda(\lambda_0, \mu_0) - \Lambda(\lambda, \mu)$ and the discretized Fréchet derivative for a given $\mathcal{B}_j$ for $j = 1, \ldots, p$, respectively. Here, we have

$$\begin{aligned}
\mathbf{V} &= (V_i)_{i=1}^{M^2} \in \mathbb{R}^{M^2}, \\
V_{(l-1)M+k} &= \Lambda_l^{(k)}(\lambda_0, \mu_0) - \Lambda_l^{(k)}(\lambda, \mu), \qquad (13) \\
\mathbf{S}^\lambda &= (S^\lambda_{ij}) \in \mathbb{R}^{M^2, p}, \\
S^\lambda_{(l-1)M+k,j} &= \int_{\mathcal{B}_j} \left(\nabla \cdot u^{(k)}_{(\lambda_0,\mu_0)}\right)\left(\nabla \cdot u^{(l)}_{(\lambda_0,\mu_0)}\right) dx, \qquad (14) \\
\mathbf{S}^\mu &= (S^\mu_{ij}) \in \mathbb{R}^{M^2, p}, \\
S^\mu_{(l-1)M+k,j} &= \int_{\mathcal{B}_j} 2\left(\hat{\nabla} u^{(k)}_{(\lambda_0,\mu_0)}\right) : \left(\hat{\nabla} u^{(l)}_{(\lambda_0,\mu_0)}\right) dx. \qquad (15)
\end{aligned}$$

Solving (12) results in a standard minimization problem for the reconstruction of the unknown parameters. In order to determine suitable parameters $(\boldsymbol{\kappa}, \boldsymbol{\nu})$, we regularize the minimization problem, so that we have

$$\left\| \left(\mathbf{S}^\lambda \mid \mathbf{S}^\mu\right) \begin{pmatrix} \boldsymbol{\kappa} \\ \boldsymbol{\nu} \end{pmatrix} - \mathbf{V} \right\|_2^2 + \omega \|\boldsymbol{\kappa}\|_2^2 + \sigma \|\boldsymbol{\nu}\|_2^2 \to \min! \tag{16}$$

with ω and σ as regularization parameters. For solving this minimization problem we consider the normal equation

$$\mathbf{A}^T \mathbf{A} \begin{pmatrix} \boldsymbol{\kappa} \\ \boldsymbol{\nu} \end{pmatrix} = \mathbf{A}^T \begin{pmatrix} \mathbf{V} \\ \mathbf{0} \\ \mathbf{0} \end{pmatrix}$$

with $\mathbf{A} = \begin{pmatrix} \mathbf{S}^\lambda & \mid \mathbf{S}^\mu \\ \omega \mathbf{I} & \mid \mathbf{0} \\ \mathbf{0} & \mid \sigma \mathbf{I} \end{pmatrix}$.

Obtaining a solution for this system is memory expensive and finding two suitable parameters ω and σ can be time consuming, since we can only choose them heuristically. However, the parameter reconstruction provides good results as shown in the next part.

Numerical realization

We present a simple test model, where we consider a cube of a biological tissue with two inclusions (tumors) as depicted in Fig. 2.

The Lamé parameters of the corresponding materials are given in Table 1.

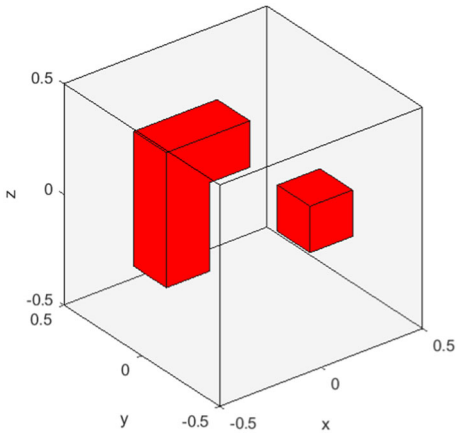

Fig. 2 Cube with two inclusions (red) as considered in [5]

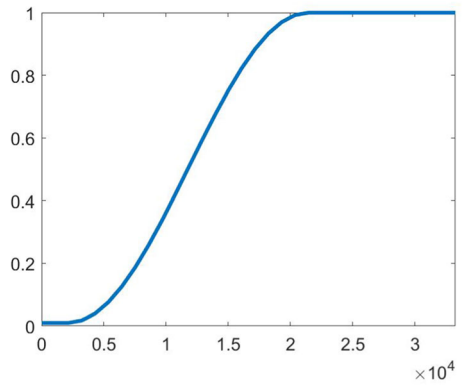

Fig. 3 Transparency function for the plots in Fig. 4 mapping the values of $|\nu|$ to $\alpha(|\nu|)$

Table 1 Lamé parameter of the test material in [Pa]

Material	λ_i	μ_i
$i = 0$: Tissue	6.6211×10^5	6.6892×10^3
$i = 1$: Tumor	2.3177×10^6	2.3411×10^4

For our numerical experiments, we simulate the discrete measurements by solving

$$\begin{cases} \nabla \cdot \left(\lambda_0(\nabla \cdot u_0)I + 2\mu_0 \hat{\nabla} u_0\right) = 0 & \text{in } \Omega, \\ -\nabla \cdot \left(((\lambda_1 - \lambda_0)\chi_D)(\nabla \cdot u_0)I + 2((\mu_1 - \mu_0)\chi_D)\hat{\nabla} u_0\right) & \\ \quad + \nabla \cdot \left(\lambda(\nabla \cdot v)I + 2\mu\hat{\nabla} v\right) = 0 & \text{in } \Omega, \\ \left(\lambda_0(\nabla \cdot u_0)I + 2\mu_0\hat{\nabla} u_0\right) n = g_l & \text{on } \Gamma_{\mathrm{N}}, \\ \left(\lambda(\nabla \cdot v)I + 2\mu\hat{\nabla} v\right) n = 0 & \text{on } \Gamma_{\mathrm{N}}, \\ u_0 = 0 & \text{on } \Gamma_{\mathrm{D}}, \\ v = 0 & \text{on } \Gamma_{\mathrm{D}}, \end{cases} \tag{17}$$

for each of the $l = 1, \ldots, M$, given boundary forces g_l, where $v := u_0 - u$ are the difference measurements. The equations regarding v in the system (17) result from substracting the boundary value problem (1) for the respective Lamé parameters.

We want to remark that the Dirichlet boundary is set to the bottom of the cube. The remaining five faces of the cube constitute the Neumann boundary. Each Neumann face is divided into 25 squares of equal size (5×5) resulting in 125 patches $\Gamma_{\mathrm{N}}^{(l)}$. On each $\Gamma_{\mathrm{N}}^{(l)}$, $l = 1, \ldots, 125$, we apply a boundary force g_l, which is equally distributed on $\Gamma_{\mathrm{N}}^{(l)}$ and pointing in the normal direction of the patch.

Exact data

First of all, we take a look at the example without noise, which means we assume we are given exact data.

In order to obtain a suitable visualization of the 3D reconstruction, we manipulate the transparency parameter function $\alpha : \mathbb{R} \to [0, 1]$ of Fig. 4 as exemplary depicted for the Lamé parameter μ in Fig. 3. It should be noted that a low transparency parameter indicates that the corresponding color (here, the colors around zero) are plotted with high transparency, while a high α indicates that the corresponding color is plotted opaque. The reason for this choice is that values of the calculated difference $\nu = \mu - \mu_0$ close to zero are not an indication of an inclusion, while values with a higher absolute value indicate an inclusion. Hence, this choice of transparency is suitable to plot the calculated inclusions without being covered by white tetrahedrons with values close to zero. Further, the reader should observe that $\alpha(|\nu|) > 0$ for all values of ν, so that all tetrahedrons are plotted and that the transparency plot for κ takes the same shape but is adjusted to the range of the calculated values.

The following results (Figs. 4 and 5) are based on a parameter search and the regularization parameters are chosen heuristically. Thus, we only present the results with the best parameter choice ($\omega = 10^{-17}$ and $\sigma = 10^{-13}$) and reconstruct the difference in the Lamé parameters μ and λ.

With these regularization parameters, the two inclusions are detected and reconstructed correctly for μ (see Fig. 4 in the left hand side) and the value of $\mu - \mu_0$ is in the correct amplitude range as depicted in Fig. 5. Figure 4 shows us, that for $\lambda - \lambda_0$, the reconstruction does not work. The reason is that the range of the Lamé parameters differs from each other around 10^2 Pa ($\lambda \approx 100 \cdot \mu$), but

$$\|\mathbf{S}^{\mu}\|_2 \approx 1.2 \cdot 10^4 \|\mathbf{S}^{\lambda}\|_2,$$

i.e. the signatures of μ are represented far stronger in the calculation of $\mathbf{V}$ than those of λ.

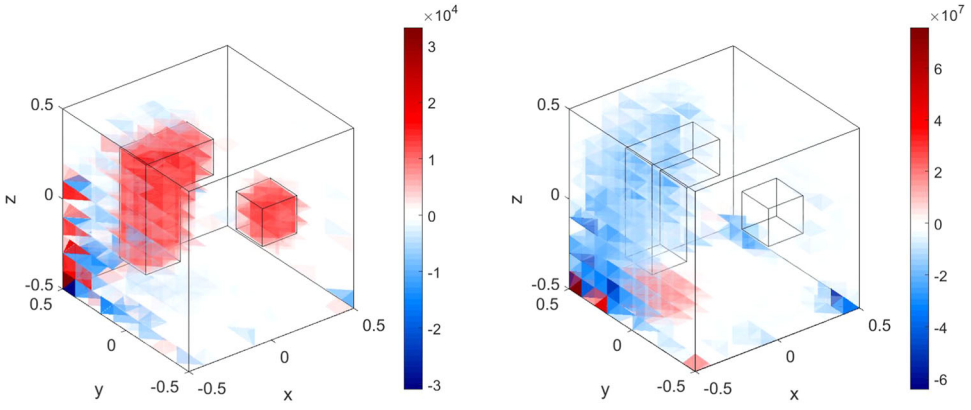

Fig. 4 Shape reconstruction of two inclusions of the difference in the Lamé parameter μ (left hand side) and λ (right hand side) for the regularization parameters $\omega = 10^{-17}$ and $\sigma = 10^{-13}$ without noise and transparency function α as shown in Fig. 3

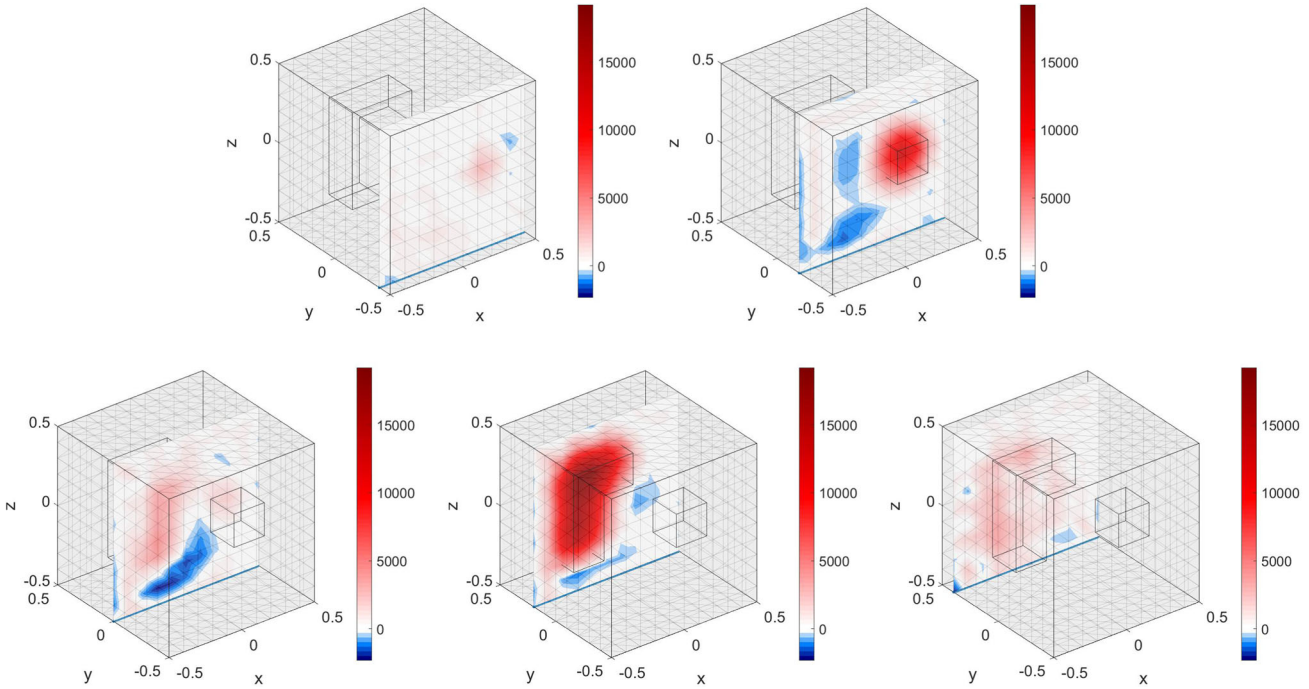

Fig. 5 Shape reconstruction of two inclusions of the reconstructed difference in the Lamé parameter μ for the regularization parameters $\omega = 10^{-17}$ and $\sigma = 10^{-13}$ depicted as cuts without noise

Noisy data

Next, we go over to noisy data. We assume that we are given a noise level $\eta \geq 0$ and set

$$\delta = \eta \cdot ||\mathbf{\Lambda}(\lambda, \mu)||_F. \tag{18}$$

Further, we define $\mathbf{\Lambda}^\delta(\lambda, \mu)$ as

$$\mathbf{\Lambda}^\delta(\lambda, \mu) = \mathbf{\Lambda}(\lambda, \mu) + \delta\overline{\mathbf{E}}, \tag{19}$$

with $\overline{\mathbf{E}} = \mathbf{E}/||\mathbf{E}||_F$, where $\mathbf{E}$ consists of $M \times M$ random uniformly distributed values in $[-1, 1]$. We set

$$\mathbf{V}^\delta = \mathbf{\Lambda}(\lambda_0, \mu_0) - \mathbf{\Lambda}^\delta(\lambda, \mu).$$

Hence, we have

$$\|\mathbf{V}^\delta - \mathbf{V}\| \leq \delta.$$

In the following examples, we consider relative noise levels of $\eta = 1\%$ (Fig. 6 and 7) and $\eta = 10\%$ (Fig. 8 and 9) with respect to the Frobenius norm as given in (19), where the regularization parameters are chosen heuristically and given in the caption of the figure.

In Fig. 6, we observe that for a low noise level with $\eta = 1\%$, we obtain a suitable reconstruction of the inclusion concerning the Lamé parameter μ and the reconstruction of λ fails again.

In contrary to the low noise level ($\eta = 1\%$), Figs. 8 and 9 show us that the standard one-step linearization method

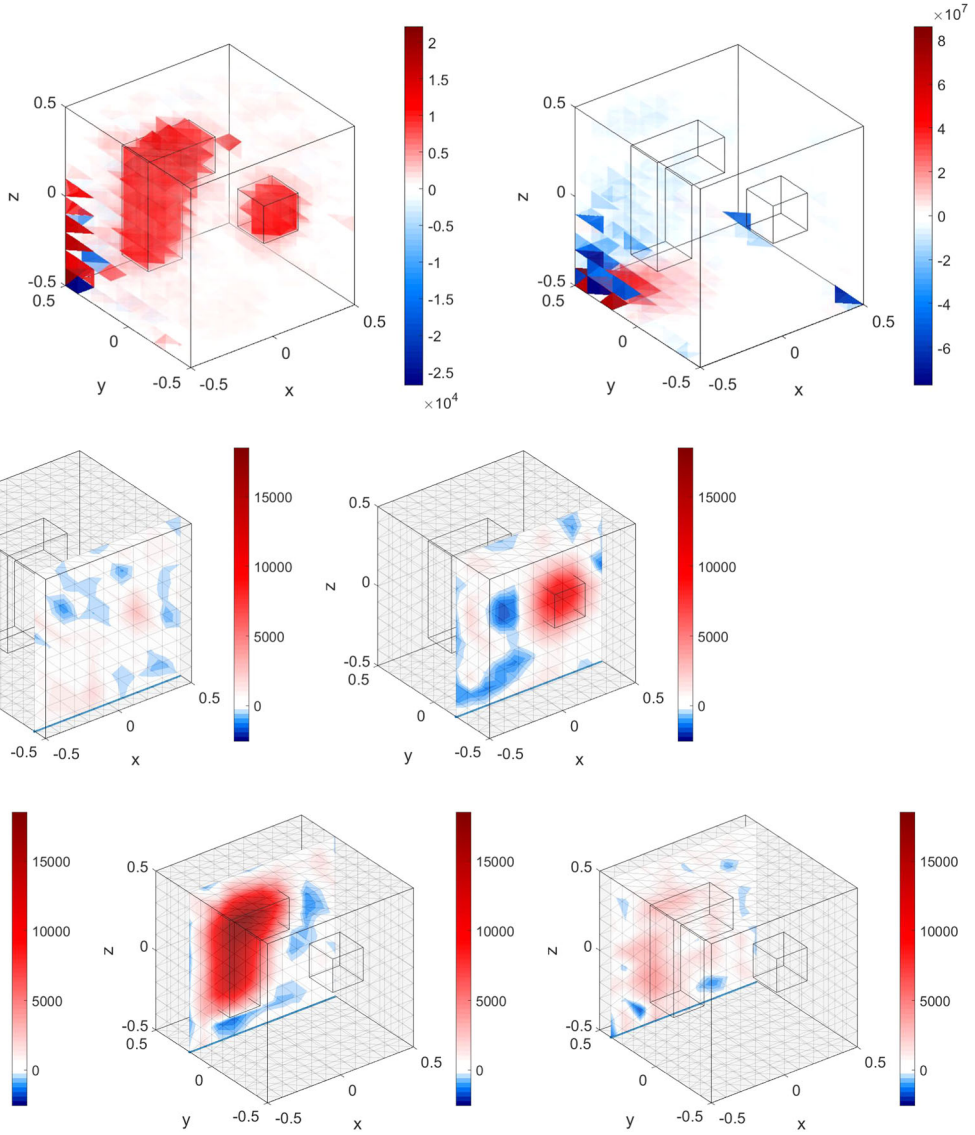

Fig. 6 Shape reconstruction of two inclusions of the difference in the Lamé parameter μ (left hand side) and λ (right hand side) for the regularization parameters $\omega = 1.1 \cdot 10^{-17}$ and $\sigma = 1.1 \cdot 10^{-13}$ with relative noise $\eta = 1\%$ and transparency function α as shown in Fig. 3

Fig. 7 Shape reconstruction of two inclusions of the reconstructed difference in the Lamé parameter μ for the regularization parameters $\omega = 1.1 \cdot 10^{-17}$ and $\sigma = 1.1 \cdot 10^{-13}$ depicted as cuts with relative noise $\eta = 1\%$

has problems in handling higher noise levels ($\eta = 10\%$). As such, in the 3D reconstruction (see Fig. 8) it is hard to recognize the two inclusions even with respect to the Lamé parameter μ. Further on in the plots of the cuts in Fig. 9, the reconstructions of the inclusions are blurred out.

Remark 1 All in all, the numerical experiments of this section motivate the consideration of a modified minimization problem in order to obtain a stable method for noisy data as well as a good reconstruction for the Lamé parameter λ. In doing so, we will combine the idea of the standard one-step linearization with the monotonicity method.

4 Enhancing the standard residual-based minimization problem

We summarize and present the required results concerning the monotonicity properties of the Neumann-to-Dirichlet operator as well as the monotonicity methods introduced and proven in [6] and Eberle and Harrach [5].

4.1 Summary of the monotonicity methods

First, we state the monotonicity estimates for the Neumann-to-Dirichlet operator $\Lambda(\lambda, \mu)$ and denote by $u^g_{(\lambda,\mu)}$ the solution of problem (1)–(3) for the boundary load g and the Lamé parameters λ and μ.

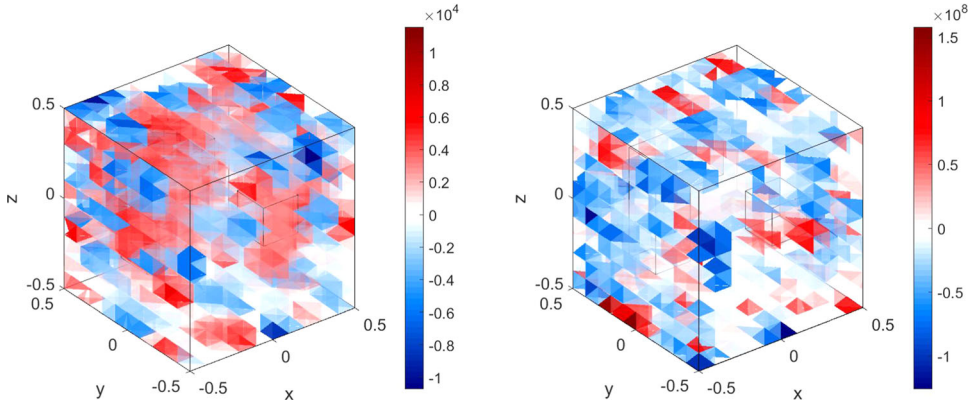

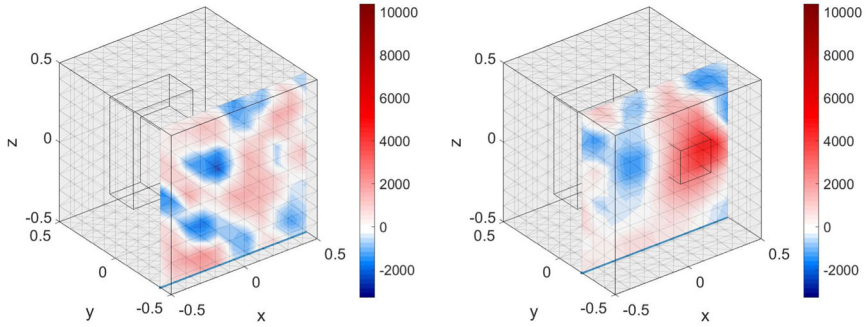

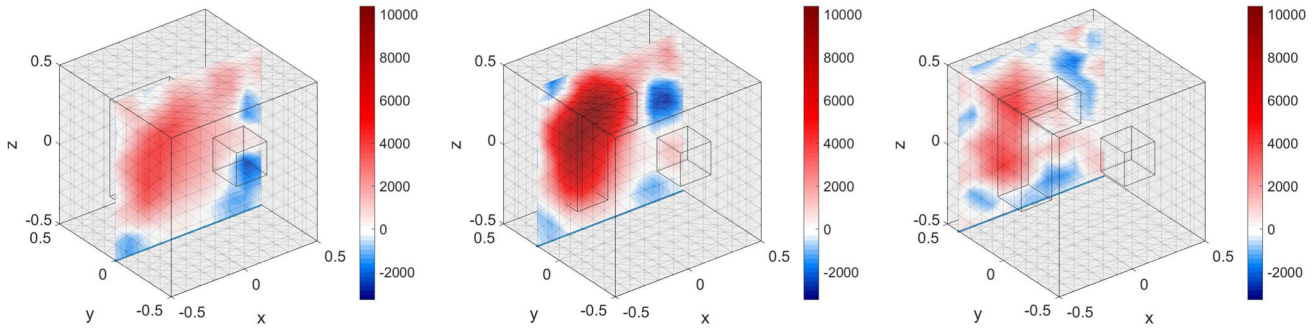

Fig. 8 Shape reconstruction of two inclusions of the difference in the Lamé parameter μ (left hand side) and λ (right hand side) for the regularization parameters $\omega = 6 \cdot 10^{-17}$ and $\sigma = 6 \cdot 10^{-13}$ with relative noise $\eta = 10\%$ and transparency function α as shown in Fig. 3

Fig. 9 Shape reconstruction of two inclusions of the reconstructed difference in the Lamé parameter μ for the regularization parameters $\omega = 6 \cdot 10^{-17}$ and $\sigma = 6 \cdot 10^{-13}$ depicted as cuts with relative noise $\eta = 10\%$

Lemma 1 (Lemma 3.1 from [6]) *Let* $(\lambda_1, \mu_1), (\lambda_2, \mu_2) \in L^\infty_+(\Omega) \times L^\infty_+(\Omega)$, $g \in L^2(\Gamma_N)^d$ *be an applied boundary force, and let* $u_1 := u^g_{(\lambda_1,\mu_1)} \in \mathcal{V}$, $u_2 := u^g_{(\lambda_2,\mu_2)} \in \mathcal{V}$. *Then*

$$\begin{aligned}
&\int_\Omega 2(\mu_1 - \mu_2)\hat{\nabla} u_2 : \hat{\nabla} u_2 + (\lambda_1 - \lambda_2)\nabla \cdot u_2 \nabla \cdot u_2 \, dx \\
&\quad \geq \langle g, \Lambda(\lambda_2, \mu_2) g\rangle - \langle g, \Lambda(\lambda_1, \mu_1) g\rangle \qquad (20) \\
&\quad \geq \int_\Omega 2(\mu_1 - \mu_2)\hat{\nabla} u_1 : \hat{\nabla} u_1 + (\lambda_1 - \lambda_2)\nabla \cdot u_1 \nabla \cdot u_1 \, dx. \qquad (21)
\end{aligned}$$

Lemma 2 (Lemma 2.2 from [5]) *Let* $(\lambda_1, \mu_1), (\lambda_2, \mu_2) \in L^\infty_+(\Omega) \times L^\infty_+(\Omega)$, $g \in L^2(\Gamma_N)^d$ *be an applied boundary force, and let* $u_1 := u^g_{(\lambda_1,\mu_1)} \in \mathcal{V}$, $u_2 := u^g_{(\lambda_2,\mu_2)} \in \mathcal{V}$. *Then*

$$\begin{aligned}
&\langle g, \Lambda(\lambda_2, \mu_2) g\rangle - \langle g, \Lambda(\lambda_1, \mu_1) g\rangle \\
&\quad \geq \int_\Omega 2\left(\mu_2 - \frac{\mu_2^2}{\mu_1}\right)\hat{\nabla} u_2 : \hat{\nabla} u_2 \, dx \\
&\qquad + \int_\Omega \left(\lambda_2 - \frac{\lambda_2^2}{\lambda_1}\right)\nabla \cdot u_2 \nabla \cdot u_2 \, dx \qquad (22) \\
&\quad = \int_\Omega 2\frac{\mu_2}{\mu_1}(\mu_1 - \mu_2)\hat{\nabla} u_2 : \hat{\nabla} u_2 \, dx \\
&\qquad + \int_\Omega \frac{\lambda_2}{\lambda_1}(\lambda_1 - \lambda_2)\nabla \cdot u_2 \nabla \cdot u_2 \, dx. \qquad (23)
\end{aligned}$$

As in the previous section, we denote by (λ_0, μ_0) the material without inclusion. Following Lemma 1, we have

Corollary 1 (Corollary 3.2 from [6]) *For* $(\lambda_0, \mu_0), (\lambda_1, \mu_1) \in L^\infty_+(\Omega) \times L^\infty_+(\Omega)$

$$\lambda_0 \leq \lambda_1 \text{ and } \mu_0 \leq \mu_1 \quad \text{implies} \quad \Lambda(\lambda_0, \mu_0) \geq \Lambda(\lambda_1, \mu_1). \tag{24}$$

Further on, we give a short overview concerning the monotonicity methods, where we restrict ourselves to the case $\lambda_1 \geq \lambda_0$, $\mu_1 \geq \mu_0$. In the following, let $\mathcal{D}$ be the unknown inclusion and $\chi_\mathcal{D}$ the characteristic function w.r.t. $\mathcal{D}$. In addition, we deal with "noisy difference measurements", i.e. distance measurements between $u^g_{(\lambda,\mu)}$ and $u^g_{(\lambda_0,\mu_0)}$ affected by noise, which stem from system (17).

We define the outer support in correspondence to Eberle and Harrach [5] as follows: let $\phi = (\phi_1, \phi_2) : \Omega \to \mathbb{R}^2$ be a measurable function, the outer support $\operatorname{out}_{\partial\Omega} \operatorname{supp}(\phi)$ is the complement (in $\overline{\Omega}$) of the union of those relatively open $U \subseteq \overline{\Omega}$ that are connected to $\partial\Omega$ and for which $\phi|_U = 0$, respectively.

Corollary 2 *Linearized monotonicity test (Corollary 2.7 from [5])*

Let $\lambda_0, \lambda_1, \mu_0, \mu_1 \in \mathbb{R}^+$ *with* $\lambda_1 > \lambda_0$, $\mu_1 > \mu_0$ *and assume that* $(\lambda, \mu) = (\lambda_0 + (\lambda_1 - \lambda_0)\chi_\mathcal{D}, \mu_0 + (\mu_1 - \mu_0)\chi_\mathcal{D})$ *with* $\mathcal{D} = \operatorname{out}_{\partial\Omega} \operatorname{supp}((\lambda - \lambda_0, \mu - \mu_0)^T)$. *Further on let* $\alpha^\lambda, \alpha^\mu \geq 0$, $\alpha^\lambda + \alpha^\mu > 0$ *and* $\alpha^\lambda \leq \frac{\lambda_0}{\lambda_1}(\lambda_1 - \lambda_0)$, $\alpha^\mu \leq \frac{\mu_0}{\mu_1}(\mu_1 - \mu_0)$. *Then for every open set* $\mathcal{B}$

$\mathcal{B} \subseteq \mathcal{D}$ *if and only if*

$$\Lambda(\lambda_0, \mu_0) + \Lambda'(\lambda_0, \mu_0)(\alpha^\lambda \chi_\mathcal{B}, \alpha^\mu \chi_\mathcal{B}) \geq \Lambda(\lambda, \mu).$$

Corollary 3 *Linearized monotonicity test for noisy data (Corollary 2.9 from [5])*

Let $\lambda_0, \lambda_1, \mu_0, \mu_1 \in \mathbb{R}^+$ *with* $\lambda_1 > \lambda_0$, $\mu_1 > \mu_0$ *and assume that* $(\lambda, \mu) = (\lambda_0 + (\lambda_1 - \lambda_0)\chi_\mathcal{D}, \mu_0 + (\mu_1 - \mu_0)\chi_\mathcal{D})$ *with* $\mathcal{D} = \operatorname{out}_{\partial\Omega} \operatorname{supp}((\lambda - \lambda_0, \mu - \mu_0)^T)$. *Further on, let* $\alpha^\lambda, \alpha^\mu \geq 0$, $\alpha^\lambda + \alpha^\mu > 0$ *with* $\alpha^\lambda \leq \frac{\lambda_0}{\lambda_1}(\lambda_1 - \lambda_0)$, $\alpha^\mu \leq \frac{\mu_0}{\mu_1}(\mu_1 - \mu_0)$. *Let* Λ^δ *be the Neumann-to-Dirichlet operator for noisy difference measurements with noise level* $\delta > 0$. *Then for every open set* $\mathcal{B} \subseteq \Omega$ *there exists a noise level* $\delta_0 > 0$, *such that for all* $0 < \delta < \delta_0$, $\mathcal{B}$ *is correctly detected as inside or not inside the inclusion* $\mathcal{D}$ *by the following monotonicity test*

$\mathcal{B} \subseteq \mathcal{D}$ *if and only if*

$$\Lambda(\lambda_0, \mu_0) + \Lambda'(\lambda_0, \mu_0)(\alpha^\lambda \chi_\mathcal{B}, \alpha^\mu \chi_\mathcal{B}) - \Lambda^\delta(\lambda, \mu) + \delta I \geq 0.$$

Finally, we present the result (see Fig. 10) obtained from noisy data Λ^δ with the linearized monotonicity method as described in Corollary 3, where we use the same pixel partition as for the one-step linearization method.

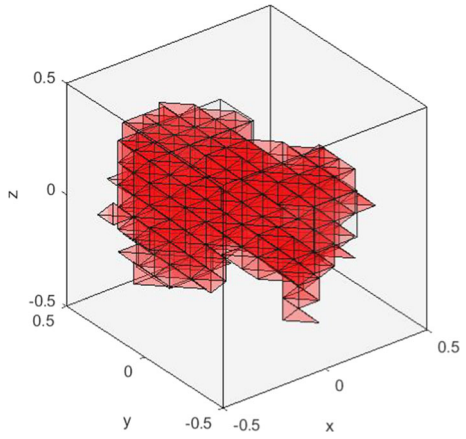

Fig. 10 Shape reconstruction of two inclusions (red) for $\alpha^\lambda = 0.28(\lambda_1 - \lambda_0) \approx 4.6 \cdot 10^5$Pa, $\alpha^\mu = 0.28(\mu_1 - \mu_0) \approx 4.7 \cdot 10^3$ Pa with relative noise $\eta = 0.1\%$ and $\delta = 1.88 \cdot 10^{-10}$

Remark 2 The linearized monotonicity method converges theoretically rigorously, but in practice delivers poorer reconstructions even for small noise (see Fig. 10, where the two inclusions are not separated) than the theoretically unproven heuristic one-step linearization (see Fig. 6, where the two inclusions are separated). Thus, we improve the standard one-step linearization method by combining it with the monotonicity method without losing the convergence results.

4.2 Monotonicity-based regularization

We assume again that the background (λ_0, μ_0) is homogeneous and that the contrasts of the anomalies $(\gamma^\lambda, \gamma^\mu)^T \in L^\infty_+(\mathcal{D})^2$ with

$$\begin{pmatrix} \lambda(x) \\ \mu(x) \end{pmatrix} = \begin{pmatrix} \lambda_0 + \gamma^\lambda(x)\chi_\mathcal{D}(x) \\ \mu_0 + \gamma^\mu(x)\chi_\mathcal{D}(x) \end{pmatrix},$$

are bounded for all $x \in \mathcal{D}$ (a.e.) via

$$c^\lambda \leq \gamma^\lambda(x) \leq C^\lambda \quad \text{and} \quad c^\mu \leq \gamma^\mu(x) \leq C^\mu,$$

with c^λ, C^λ, c^μ, $C^\mu \geq 0$. $\mathcal{D}$ is an open set denoting the anomalies and the parameters λ_0, μ_0, c^λ, c^μ, C^λ and C^μ are assumed to be known.

Remark 3 It should be noted that $\Omega \setminus \mathcal{D}$ has to be connected.

In doing so, we can also handle more general Lamé parameters and not only piecewise constant parameters as in the previous section.

Here, we focus on the case $\lambda \geq \lambda_0$, $\mu \geq \mu_0$, while the case $\lambda \leq \lambda_0$, $\mu \leq \mu_0$ can be found in the "Appendix".

Similar as in the one-step linearization method, we make the piecewise constant ansatz (11) in order to approximate $(\gamma^\lambda, \gamma^\mu)$ by (κ, ν).

The main idea of monotonicity-based regularization is to minimize the residual of the linearized problem, i.e.,

$$\left\| \left(\mathbf{S}^{\lambda} \mid \mathbf{S}^{\mu}\right) \begin{pmatrix} \boldsymbol{\kappa} \\ \boldsymbol{\nu} \end{pmatrix} - \mathbf{V} \right\|_2^2 \to \min! \tag{25}$$

with constraints on $(\boldsymbol{\kappa}, \boldsymbol{\nu})$ that are obtained from the monotonicity properties introduced in Lemma 1 and 2. Our aim is to rewrite the minimization problem (25) for the case $\mu_0 \neq \mu$, $\lambda_0 \neq \lambda$ in $\mathcal{D}$ in order to be able to reconstruct the inclusions also with respect to λ. Our intention is to force that both Lamé parameters $\mu(x)$ and $\lambda(x)$ take the same shape but different scale.

In more detail, we define the quantities $a_{\max}$ and τ as

$$a_{\max} := \mu_0 - \frac{\mu_0^2}{\mu_0 + c^{\mu}}, \tag{26}$$

$$\tau := \frac{1}{a_{\max}} \left(\lambda_0 - \frac{\lambda_0^2}{\lambda_0 + c^{\lambda}} \right), \tag{27}$$

such that

$$-2\left(\mu_0 - \frac{\mu_0^2}{\mu}\right) + 2a \leq 0, \tag{28}$$

$$-\left(\lambda_0 - \frac{\lambda_0^2}{\lambda}\right) + \tau a \leq 0 \tag{29}$$

for all $0 \leq a \leq a_{\max}$.

In addition, we set the residual $r(\nu)$ as

$$r(\nu) := \Lambda(\lambda, \mu) - \Lambda(\lambda_0, \mu_0) - \Lambda'(\lambda_0, \mu_0)(\tau\nu, \nu)$$

and the components of the corresponding matrix $\mathbf{R}(\nu)$ are given by

$$(\mathbf{R}(\nu))_{i,j=1,\dots M} := \left(\langle g_i, r(\nu) g_j \rangle\right)_{i,j=1,\dots M}.$$

We want to remark, that we use the same boundary loads g_i, $i = 1, \dots, M$, as in Sect. 2.

Finally, we introduce the set

$$\mathcal{C} := \left\{ \nu \in L^{\infty}(\Omega) : \nu = \sum_{k=1}^{p} a_k \chi_k,\ a_k \in \mathbb{R},\ 0 \leq a_k \leq \min(a_{\max}, \beta_k) \right\}$$

with

$$\beta_k := \max\left\{ a \geq 0 :\ \Lambda(\lambda, \mu) - \Lambda(\lambda_0, \mu_0) \leq \Lambda'(\lambda_0, \mu_0)(\tau a \chi_k, a\chi_k) \right\}, \tag{30}$$

where we set $\chi_k := \chi_{\mathcal{B}_k}$.

Note that the set on the right hand side of (30) is non-empty since it contains the value zero by Corollary 1 and our assumptions $\lambda \geq \lambda_0$, $\mu \geq \mu_0$.

Then, we modify the original minimization problem (25) to

$$\min_{\nu \in \mathcal{C}} \|\mathbf{R}(\nu)\|_F.$$

Remark 4 We want to remark that β_k is defined via the infinite-dimensional Neumann-to-Dirichlet operator $\Lambda(\lambda, \mu)$ and does not involve the finite dimensional matrix $\mathbf{R}$. For the numerical realization we will require a discrete version $\tilde{\beta}_k$ of β_k introduced later on.

4.2.1 Main results

In the following we present our main results and will show that the choices of the quantities $a_{\max}$ and τ will lead to the correct reconstruction of the support of $\kappa(x)$ and $\nu(x)$, which we introduced in (26) and (27), respectively, based on the lower bounds from the monotonicity tests as stated in (28) and (29).

Theorem 1 *Consider the minimization problem*

$$\min_{\nu \in \mathcal{C}} \|\mathbf{R}(\nu)\|_F. \tag{31}$$

The following statements hold true:

(i) Problem (31) admits a unique minimizer $\hat{\nu}$.

(ii) $\operatorname{supp}(\hat{\nu})$ *and* $\mathcal{D}$ *agree up to the pixel partition, i.e. for any pixel* $\mathcal{B}_k$

$$\mathcal{B}_k \subset \operatorname{supp}(\hat{\nu}) \quad \textit{if and only if} \quad \mathcal{B}_k \subset \mathcal{D}.$$

Moreover,

$$\hat{\nu} = \sum_{\mathcal{B}_k \subseteq \mathcal{D}} a_{\max} \chi_k.$$

Now we deal with noisy data and introduce the corresponding residual

$$r_{\delta}(\nu) := \Lambda^{\delta}(\lambda, \mu) - \Lambda(\lambda_0, \mu_0) - \Lambda'(\lambda_0, \mu_0)(\tau\nu, \nu). \tag{32}$$

Based on this, $\mathbf{R}_{\delta}(\nu)$ represents the matrix $(\langle g_i, r_{\delta}(\nu) g_j \rangle)_{i,j=1,\dots M}$.

Further on, the admissible set for noisy data is defined by

$$\mathcal{C}_{\delta} := \left\{ \nu \in L^{\infty}(\Omega) : \nu = \sum_{k=1}^{p} a_k \chi_k,\ a_k \in \mathbb{R},\ 0 \leq a_k \leq \min(a_{\max}, \beta_{k,\delta}) \right\}$$

with

$$\beta_{k,\delta} := \max\left\{a \geq 0 :\ \Lambda^{\delta}(\lambda,\mu) - \Lambda(\lambda_0,\mu_0) - \delta I \leq \Lambda'(\lambda_0,\mu_0)(\tau a\chi_k, a\chi_k)\right\}. \tag{33}$$

Thus, we present the following stability result.

Theorem 2 *Consider the minimization problem*

$$\min_{\nu\in\mathcal{C}_\delta} \|\mathbf{R}_\delta(\nu)\|_F. \tag{34}$$

The following statements hold true:

(i) Problem (34) admits a minimizer.
(ii) Let $\hat{\nu} = \sum_{\mathcal{B}_k\subseteq\mathcal{D}} a_{\max}\chi_k$ *be the minimizer of (31) and* $\hat{\nu}_\delta = \sum_{k=1}^{p} a_{k,\delta}\chi_k$ *of problem (34), respectively. Then* $\hat{\nu}_\delta$ *converges pointwise and uniformly to* $\hat{\nu}$ *as* δ *goes to* 0.

Remark 5 In [5], we used monotonicity methods to solve the inverse problem of shape reconstruction. In Theorems 1 and 2, we applied the same monotonicity methods to construct constraints for the residual based inversion technique. Both methods have a rigorously proven convergence theory, however the monotonicity-based regularization approach turns out to be more stable regarding noise.

4.2.2 Theoretical background

In order to prove Theorem 1 as well as Theorem 2, we have to take a look at the following.

Lemma 3 *Let* $a_{\max}$ *and* τ *be defined as in (26) and (27), respectively,* $\lambda,\mu \in L^\infty_+(\Omega)$ *and we assume that* $\lambda \geq \lambda_0$, $\mu \geq \mu_0$, *where* λ_0,μ_0 *are constant. Then we have for any pixel* $\mathcal{B}_k$, $\mathcal{B}_k \subseteq \mathcal{D}$ *if and only if* $\beta_k > 0$, *where* β_k *is defined in (30).*

Proof We adopt the proof of Lemma 3.4 from [11].
Step 1: First, we verify that from $\mathcal{B}_k \subseteq \mathcal{D}$ it follows that $\beta_k > 0$.

In fact, by applying the monotonicity principle (22) multiplied by -1 for

$$\lambda_1 := \lambda, \mu_1 := \mu \ \text{ and } \ \lambda_2 := \lambda_0, \mu_2 := \mu_0,$$

we end up with the following inequalities for all pixel $\mathcal{B}_k$, all $a \in [0, a_{\max}]$ and all $g \in L^2(\Gamma_N)^d$

$$\begin{aligned}
&\left\langle g, \left(\Lambda(\lambda,\mu) - \Lambda(\lambda_0,\mu_0) - \Lambda'(\lambda_0,\mu_0)(\tau a\chi_k, a\chi_k)\right) g\right\rangle \\
&\leq -\int_\Omega 2\left(\mu_0 - \frac{\mu_0^2}{\mu}\right)\hat{\nabla}u_0^g : \hat{\nabla}u_0^g\,dx + \int_\Omega 2a\chi_k\hat{\nabla}u_0^g : \hat{\nabla}u_0^g\,dx \\
&\quad - \int_\Omega\left(\lambda_0 - \frac{\lambda_0^2}{\lambda}\right)\nabla\cdot u_0^g\nabla\cdot u_0^g\,dx + \int_\Omega \tau a\chi_k\nabla\cdot u_0^g\nabla\cdot u_0^g\,dx \\
&\leq -\int_{\mathcal{D}} 2\left(\mu_0 - \frac{\mu_0^2}{\mu}\right)\hat{\nabla}u_0^g : \hat{\nabla}u_0^g\,dx + \int_{\mathcal{B}_k} 2a_{\max}\hat{\nabla}u_0^g : \hat{\nabla}u_0^g\,dx \\
&\quad - \int_{\mathcal{D}}\left(\lambda_0 - \frac{\lambda_0^2}{\lambda}\right)\nabla\cdot u_0^g\nabla\cdot u_0^g\,dx + \int_{\mathcal{B}_k}\tau a_{\max}\nabla\cdot u_0^g\nabla\cdot u_0^g\,dx \\
&\leq 0.
\end{aligned}$$

In the above inequalities, we used the shorthand notation u_0^g for the unique solution $u^g_{(\lambda_0,\mu_0)}$. The last inequality holds due to the fact that $a_{\max}$ and τ fulfill

$$\begin{aligned}
&-2\left(\mu_0 - \frac{\mu_0^2}{\mu}\right) + 2a_{\max} \leq 0, \\
&-\left(\lambda_0 - \frac{\lambda_0^2}{\lambda}\right) + \tau a_{\max} \leq 0
\end{aligned}$$

in $\mathcal{D}$ and that $\mathcal{B}_k$ lies inside $\mathcal{D}$.

We want to remark, that compared with the corresponding proof in Harrach and Mach [11], this shows us that we require conditions on $a_{\max}$ as well as on τ (c.f. Eq. (28) and (29)) due to the fact that we deal with two unknown parameters (λ and μ) instead of one.

Step 2: In order to prove the other direction of the statement, let $\beta_k > 0$. We will show that $\mathcal{B}_k \subseteq \mathcal{D}$ by contradiction.

Assume that $\mathcal{B}_k \nsubseteq \mathcal{D}$ and $\beta_k > 0$. Applying the monotonicity principle from Lemma 1,

$$\Lambda(\lambda,\mu) - \Lambda(\lambda_0,\mu_0) \geq \Lambda'(\lambda_0,\mu_0)((\lambda,\mu) - (\lambda_0,\mu_0)),$$

with the definition of β_k in (30), we are led to

$$\begin{aligned}
0 &\geq \Lambda(\lambda,\mu) - \Lambda(\lambda_0,\mu_0) - \Lambda'(\lambda_0,\mu_0)(\tau\beta_k\chi_k, \beta_k\chi_k) \\
&\geq \Lambda'(\lambda_0,\mu_0)((\lambda,\mu) - (\lambda_0,\mu_0)) \\
&\quad - \Lambda'(\lambda_0,\mu_0)(\tau\beta_k\chi_k, \beta_k\chi_k).
\end{aligned}$$

Based on this, we conclude that for all $g \in L^2(\Gamma_N)^d$

$$\begin{aligned}
&\int_{\mathcal{B}_k}\tau\beta_k\nabla\cdot u_0^g\nabla\cdot u_0^g\,dx + 2\int_{\mathcal{B}_k}\beta_k\hat{\nabla}u_0^g : \hat{\nabla}u_0^g\,dx \\
&\leq \int_\Omega(\lambda-\lambda_0)\nabla\cdot u_0^g\nabla\cdot u_0^g\,dx + 2\int_\Omega(\mu-\mu_0)\hat{\nabla}u_0^g : \hat{\nabla}u_0^g\,dx \\
&\leq \int_{\mathcal{D}} C^\lambda\nabla\cdot u_0^g\nabla\cdot u_0^g\,dx + 2\int_{\mathcal{D}} C^\mu\hat{\nabla}u_0^g : \hat{\nabla}u_0^g\,dx.
\end{aligned} \tag{35}$$

On the other hand, using the localized potentials in a similar procedure as in the proof of Theorem 2.1 in [5], we can find a sequence $(g_m)_{m\in\mathbb{N}} \subset L^2(\Gamma_N)^d$ such that the solutions $(u_0^m)_{m\in\mathbb{N}} \subset H^1(\Omega)^d$ of the forward problem (when the Lamé parameter are chosen to be λ_0, μ_0 and the boundary forces $g = g_m$) fulfill

$$\lim_{m\to\infty}\int_{\mathcal{B}_k}\hat{\nabla}u_0^m : \hat{\nabla}u_0^m\,dx = \infty, \qquad \lim_{m\to\infty}\int_{\mathcal{D}}\hat{\nabla}u_0^m : \hat{\nabla}u_0^m\,dx = 0,$$

$$\lim_{m\to\infty}\int_{\mathcal{B}_k}\nabla\cdot u_0^m\nabla\cdot u_0^m\,dx=\infty,\quad \lim_{m\to\infty}\int_{\mathcal{D}}\nabla\cdot u_0^m\nabla\cdot u_0^m\,dx=0,$$

which contradicts (35). □

Lemma 4 *For all pixels $\mathcal{B}_k$, denote by $\mathbf{S}_k^\tau$ the matrix*

$$\mathbf{S}_k^\tau:=\left(\langle g_i,-\Lambda'(\lambda_0,\mu_0)(\tau\chi_k,\chi_k)g_j\rangle\right)_{i,j=1,\dots,M}.$$

Then $\mathbf{S}_k^\tau$ is a positive definite matrix.

Proof We adopt the proof of Lemma 3.5 from [11] for the matrix $\mathbf{S}_k^\tau$, which directly yields the desired result. □

Proof (**Theorem** 1) This proof is based on the proof of Theorem 3.2 from [11].

to (i) Since the functional

$$v\mapsto\|\mathbf{R}(v)\|_F^2:=\sum_{i,j=1}^{M}\langle g_i,r(v)g_j\rangle^2$$

is continuous, it admits a minimizer in the compact set $\mathcal{C}$.

The uniqueness of $\hat{v}$ will follow from the proof of (ii) *Step 3*.

to (ii) *Step 1* We shall check that for all

$$v=\sum_{k=1}^{p}a_k\chi_k\quad\text{satisfying}\quad 0\le a_k\le\min(a_{\max},\beta_k),$$

it holds that $r(v)\le 0$ in quadratic sense. We want to remark that for $a_{\max}$ and τ the inequalities (28) and (29) hold in $\mathcal{D}$.

We proceed similar as in the proof of Lemma 3 and use Lemma 2 for $\lambda_1=\lambda,\mu_1=\mu,\lambda_2=\lambda_0$ and $\mu_2=\mu_0$. In addition, we multiply the whole expression with -1. Thus, it holds that

$$\begin{aligned}&\langle g,(\Lambda(\lambda,\mu)-\Lambda(\lambda_0,\mu_0)-\Lambda'(\lambda_0,\mu_0)(\tau v,v))g\rangle\\&\le-\int_{\mathcal{D}}2a_{\max}\hat{\nabla}u_0^g:\hat{\nabla}u_0^g\,dx+\sum_{k=1}^{p}\int_{\mathcal{B}_k}2a_k\hat{\nabla}u_0^g:\hat{\nabla}u_0^g\,dx\\&\quad-\int_{\mathcal{D}}\tau a_{\max}\nabla\cdot u_0^g\nabla\cdot u_0^g\,dx+\sum_{k=1}^{p}\int_{\mathcal{B}_k}\tau a_k\nabla\cdot u_0^g\nabla\cdot u_0^g\,dx\end{aligned}$$

for any $g\in L^2(\Gamma_N)^d$.

If $a_k>0$, it follows $\beta_k\ge a_k>0$, so that Lemma 3 implies that $\mathcal{B}_k\subseteq\mathcal{D}$. Since $a_k\le a_{\max}$, we end up with $\langle g,r(v)g\rangle\le 0$ for $g\in L^2(\Gamma_N)^d$.

Step 2: Let $\hat{v}=\sum_{k=1}^{p}\hat{a}_k\chi_k$ be a minimizer of problem (31). We show that $\operatorname{supp}(\hat{v})\subseteq\mathcal{D}$.

Per definition of β_k, it holds that $\beta_k\ge\hat{a}_k$. This implies $\beta_k>0$. With Lemma 3 we have $\mathcal{B}_k\subseteq\mathcal{D}$.

Step 3: We will prove that, if $\hat{v}=\sum_{k=1}^{p}\hat{a}_k\chi_k$ is a minimizer of problem (31), then the representation of $\hat{a}_k$ is given by

$$\hat{a}_k=\begin{cases}0 & \text{for } \mathcal{B}_k\not\subseteq\mathcal{D},\\ a_{\max} & \text{for } \mathcal{B}_k\subseteq\mathcal{D}.\end{cases}$$

In fact, it holds that $\hat{a}_k<a_{\max}$. If there exists a pixel $\mathcal{B}_k$ such that $\hat{v}(x)<\min(a_{\max},\beta_k)$ in $\mathcal{B}_k$, we can choose $h^v>0$, such that $\hat{v}+h^v\chi_k=a_{\max}$ in $\mathcal{B}_k$. We will show that then,

$$\|\mathbf{R}(\hat{v}+h^v\chi_k)\|_F<\|\mathbf{R}(\hat{v})\|_F,$$

which contradicts the minimality of $\hat{v}$. Thus, it follows that $\hat{a}_k=\min(a_{\max},\beta_k)$.

To show the contradiction, let $\theta_1(\hat{v})\ge\theta_2(\hat{v})\ge\cdots\ge\theta_M(\hat{v})$ be M eigenvalues of $\mathbf{R}(\hat{v})$ and $\theta_1(\hat{v}+h^v\chi_k)\ge\theta_2(\hat{v}+h^v\chi_k)\ge\cdots\ge\theta_M(\hat{v}+h^v\chi_k)$ M eigenvalues of $\mathbf{R}(\hat{v}+h^v\chi_k)$.

Since $\mathbf{R}(\hat{v})$ and $\mathbf{R}(\hat{v}+h^v\chi_k)$ are both symmetric, all of their eigenvalues are real. By the definition of the Frobenius norm, we obtain

$$\begin{aligned}&\|\mathbf{R}(\hat{v}+h^v\chi_k)\|_F^2-\|\mathbf{R}(\hat{v})\|_F^2\\&=\sum_{i=1}^{M}|\theta_i(\hat{v}+h^v\chi_k)|^2-\sum_{i=1}^{M}|\theta_i(\hat{v})|^2\\&=\sum_{i=1}^{M}\left(\theta_i\left(\hat{v}+h^v\chi_k\right)+\theta_i(\hat{v})\right)\cdot\left(\theta_i(\hat{v}+h^v\chi_k)-\theta_i(\hat{v})\right).\end{aligned}$$

Due to *Step 1*, $r(\hat{v})\le 0$ and $r(\hat{v}+h^v\chi_k)\le 0$ in the quadratic sense. Thus, for all $x=(x_1,\dots,x_M)^T\in\mathbb{R}^M$, we have

$$x^T\mathbf{R}(\hat{v})x=\sum_{i,j=1}^{M}x_ix_j\langle g_i,r(\hat{v})g_j\rangle=\langle g,r(\hat{v})g\rangle\le 0,$$

where $g=\sum_{i=1}^{M}x_ig_i$. This means that $-\mathbf{R}(\hat{v})$ is a positive semi-definite symmetric matrix in $\mathbb{R}^{M\times M}$. Due to the fact, that all eigenvalues of a positive semi-definite symmetric matrix are non-negative, it follow that $\theta_i(\hat{v})\le 0$ for all $i\in\{1,\dots,M\}$. By the same considerations, $-\mathbf{R}(\hat{v}+h^v\chi_k)$ is also a positive semi-definite matrix. We want to remark, that $\mathbf{S}_k^\tau$ is positive definite as proven in Lemma 4 and hence, all M eigenvalues of $\theta_1(\mathbf{S}_k^\tau)\ge\cdots\ge\theta_M(\mathbf{S}_k^\tau)$ are positive. Since

$$\mathbf{R}(\hat{v}+h^v\chi_k)=\mathbf{R}(\hat{v})+h^v\mathbf{S}_k^\tau$$

and the matrices $\mathbf{R}(\hat{v}+h^v\chi_k)$, $\mathbf{R}(\hat{v})+h^v$ and $\mathbf{S}_k^\tau$ are symmetric, we can apply Weyl's Inequalities to get

$$\theta_i(\hat{v}+h^v\chi_k)\ge\theta_i(\hat{v})+\theta_M(h^v\mathbf{S}_k^\tau)>\theta_i(\hat{v})$$

for all $i\in\{1,\dots,M\}$.

In summary we end up with

$$\|\mathbf{R}(\hat{v} + h^{\nu}\chi_k)\|_F < \|\mathbf{R}(\hat{v})\|_F,$$

which contradicts the minimality of $\hat{v}$ and thus, ends the proof of *Step 3*.

Step 4: We show that, if $\mathcal{B}_k \subseteq \mathcal{D}$, then $\mathcal{B}_k \subseteq \text{supp}(\hat{v})$. Indeed, since $\hat{v}$ is a minimizer of problem (31), *Step 3* implies that

$$\hat{v} = \sum_{k=1}^{p} \min(a_{\max}, \beta_k)\chi_k.$$

Since $\mathcal{B}_k \subseteq \mathcal{D}$, it follows from Lemma 3 that $\min(a_{\max}, \beta_k) > 0$. Thus, $\mathcal{B}_k \subseteq \text{supp}(\hat{v})$.

In conclusion, problem (31) admits a unique minimizer $\hat{v}$ with

$$\hat{v} = \sum_{k=1}^{p} \min(a_{\max}, \beta_k)\chi_k.$$

This minimizer fulfills

$$\hat{v} = \begin{cases} a_{\max} & \text{in } \mathcal{B}_k, \quad \text{if } \mathcal{B}_k \text{ lies inside } \mathcal{D}, \\ 0 & \text{in } \mathcal{B}_k, \quad \text{if } \mathcal{B}_k \text{ does not lie inside } \mathcal{D}, \end{cases}$$

so that

$$\hat{v} = \sum_{\mathcal{B}_k \subseteq \mathcal{D}} a_{\max}\chi_k.$$

□

Next, we go over to noisy data and take a look at the following lemma, where we set $V^{\delta} := \frac{1}{2}(V^{\delta} + (V^{\delta})^*)$, since we always can redefine the data V^{δ} in this way without loss of generality. Thus, we can assume that V^{δ} is self-adjoint.

Lemma 5 *Assume that $\|\Lambda^{\delta}(\lambda, \mu) - \Lambda(\lambda, \mu)\| \leq \delta$. Then for every pixel $\mathcal{B}_k$, it holds that $\beta_k \leq \beta_{k,\delta}$ for all $\delta > 0$.*

Proof The proof follows the lines of Lemma 3.7 in [11] with the following modifications. We have to check that β_k as given in (30) fulfills the relation

$$|V^{\delta}| + \Lambda'(\lambda_0, \mu_0)(\tau a\chi_k, a\chi_k) \geq -\delta I \quad \text{for all } a \in [0, \beta_k],$$

where $|V^{\delta}| = \sqrt{(V^{\delta})^* V^{\delta}}$.

As proven in [11], $V - V^{\delta} \geq -\delta I$ in quadratic sense. Further on Lemma 3.6 from [11] implies $|V^{\delta}| \geq V^{\delta}$, since V^{δ} is self-adjoint. Hence,

$$\begin{aligned} &|V^{\delta}| + \Lambda'(\lambda_0, \mu_0)(\tau\beta_k\chi_k, \beta_k\chi_k) \\ &\quad \geq V^{\delta} + \Lambda'(\lambda_0, \mu_0)(\tau\beta_k\chi_k, \beta_k\chi_k) \\ &\quad = V + \Lambda'(\lambda_0, \mu_0)(\tau\beta_k\chi_k, \beta_k\chi_k) + V^{\delta} - V \\ &\quad \geq -\delta I. \end{aligned}$$

□

Remark 6 As a consequence, it holds that

1. If $\mathcal{B}_k$ lies inside $\mathcal{D}$, then $\beta_{k,\delta} \geq a_{\max}$.
2. If $\beta_{k,\delta} = 0$, then $\mathcal{B}_k$ does not lie inside $\mathcal{D}$.

Proof **(Theorem 2)** This proof is based on the proof of Theorem 3.8 in [11].

to (i) For the proof of the existence of a minimizer of (34), we argue as in the proof of Theorem 1 (i). First, we take a look at the functional

$$\nu \mapsto \|\mathbf{R}_{\delta}(\nu)\|_F^2, \tag{36}$$

which is defined by $(\mathbf{R}_{\delta}(\nu))_{i,j=1,\dots M} := \big(\langle g_i, r_{\delta}(\nu)g_j\rangle\big)_{i,j=1,\dots M}$ via the residual (32). Since the functional (36) is continuous, it follows that there exists at least one minimizer in the compact set $\mathcal{C}_{\delta}$.

to (ii) *Step 1:* Convergence of a subsequence of $\hat{v}_{\delta}$

For any fixed k, the sequence $\{\hat{a}_{k,\delta}\}_{\delta>0}$ is bounded from below by 0 and from above by $a_{\max}$, respectively. By Weierstrass' Theorem, there exists a subsequence $(\hat{a}_{1,\delta_n}, \dots, \hat{a}_{p,\delta_n})$ converging to some limit $(a_1, \dots, a_p)$. Of course, $0 \leq a_k \leq a_{\max}$ for all $k = 1, \dots, p$.

Step 2: Upper bound and limit

We shall check that $a_k \leq \beta_k$ for all $k = 1, \dots, p$. As shown in the proof of Theorem 3.8 in [11], $|V^{\delta}|$ converges to $|V|$ in the operator norm as δ goes to 0, and hence, for any fixed k,

$$\begin{aligned} &|V| + \Lambda'(\lambda_0, \mu_0)(\tau a_k\chi_k, a_k\chi_k) \\ &\quad = \lim_{\delta_n \to 0} (|V^{\delta_n}| + \Lambda'(\lambda_0, \mu_0)(\tau\hat{a}_{k,\delta_n}\chi_k, \hat{a}_{k,\delta_n}\chi_k)) \end{aligned}$$

in the operator norm. As in [11], we obtain that for all $g \in L^2(\Gamma_N)^d$,

$$\langle g, (|V| + \Lambda'(\lambda_0, \mu_0)(\tau a_k\chi_k, a_k\chi_k))g\rangle \geq 0.$$

Step 3: Minimality of the limit

Due to Lemma 5, we know that $\min(a_{\max}, \beta_k) \leq \min(a_{\max}, \beta_{k,\delta})$ for all $k = 1, \dots, p$. Thus, $\hat{v}$ belongs to the admissible set $\mathcal{C}_{\delta}$ of the minimization problem (34) for all $\delta > 0$. By minimality of $\hat{v}_{\delta}$, we obtain

$$\|\mathbf{R}_{\delta}(\hat{v}_{\delta})\|_F \leq \|\mathbf{R}_{\delta}(\hat{v})\|_F.$$

Denote by $\nu = \sum_{k=1}^{p} a_k \chi_k$, where a_k are the limits derived in *Step 1*. We have that

$$\|\mathbf{R}_{\delta_n}(\hat{v}_{\delta_n})\|_F^2 = \sum_{i,j=1}^{M} \left\langle g_i, \left(-V^{\delta_n} - \sum_{k=1}^{p} \Lambda'(\lambda_0, \mu_0)(\tau \hat{a}_{k,\delta_n} \chi_k, \hat{a}_{k,\delta_n} \chi_k)\right) g_j \right\rangle^2,$$

$$\|\mathbf{R}(\nu)\|_F^2 = \sum_{i,j=1}^{M} \left\langle g_i, \left(-V - \sum_{k=1}^{p} \Lambda'(\lambda_0, \mu_0)(\tau a_k \chi_k, a_k \chi_k)\right) g_j \right\rangle^2.$$

With the same arguments as in the proof of Theorem 3.8 in [11], i.e. that V converges to V^δ as well as $\hat{a}_{k,\delta}$ goes to a_k, we are led to

$$\|\mathbf{R}(\nu)\|_F \leq \|\mathbf{R}(\hat{\nu})\|_F.$$

Further on, by the uniqueness of the minimizer we obtain $\nu = \hat{\nu}$ that is

$$a_k = \hat{a}_k = \begin{cases} 0 & \text{for } \mathcal{B}_k \not\subseteq \mathcal{D}, \\ a_{\max} & \text{for } \mathcal{B}_k \subseteq \mathcal{D}. \end{cases}$$

Step 4: Convergence of the whole sequence $\hat{\nu}_\delta$

Again this is obtained in the same way as in [11] and is based on the knowledge that every subsequence of $(\hat{a}_{1,\delta}, \ldots, \hat{a}_{p,\delta})$ possesses a convergent subsubsequence, that goes to the limit $(\min(a, \beta_1), \ldots, \min(a, \beta_p))$. □

Remark 7 All in all, we are led to the discrete formulation of the minimization problem for noisy data:

$$\min_{\nu \in \mathcal{C}_\delta} \|\mathbf{R}_\delta(\nu)\|_F, \tag{37}$$

under the constraint

$$0 \leq \nu_k \leq \min\left(a_{\max}, \tilde{\beta}_{k,\delta}\right), \tag{38}$$

where

$$a_{\max} = \mu_0 - \frac{\mu_0^2}{\mu_0 + c^\mu}, \tag{39}$$

$$\tau = \frac{1}{a_{\max}} \left(\lambda_0 - \frac{\lambda_0^2}{\lambda_0 + c^\lambda}\right), \tag{40}$$

$$\tilde{\beta}_{k,\delta} = \max\{a \geq 0 \,:\, -a\mathbf{S}_k^\tau \geq -\delta\mathbf{I} - |\mathbf{V}^\delta|\} \tag{41}$$

with $|\mathbf{V}^\delta| := \sqrt{(\mathbf{V}^\delta)^* \mathbf{V}^\delta}$.

We want to mention, that $\mathbf{V}$ is positive definite, however, $\mathbf{V}^\delta$ is not in general, which leads to problems in the proofs. Hence, we use $|\mathbf{V}^\delta|$ instead.

Next, we take a closer look at the determination of $\tilde{\beta}_{k,\delta}$ (see [11]), where $\tilde{\beta}_{k,0} = \tilde{\beta}_k$:

Table 2 Lower and upper bounds c^λ, c^μ, C^λ, C^μ in [Pa]

	γ^λ	γ^μ
Lower bounds	$c^\lambda = 1.2 \times 10^6$	$c^\mu = 1.2 \times 10^4$
Upper bounds	$C^\lambda = 1.7 \times 10^6$	$C^\mu = 1.7 \times 10^4$

First, we replace the infinite-dimensional operators $|V^\delta|$ and $\Lambda'(\lambda_0, \mu_0)$ in (33) by the $M \times M$ matrices $\mathbf{V}^\delta$, $\mathbf{S}_k^\tau$ such that we need to find $\tilde{\beta}_{k,\delta}$ with

$$-a\mathbf{S}_k^\tau \geq -\delta\mathbf{I} - |\mathbf{V}^\delta|$$

for all $a \in [0, \tilde{\beta}_{k,\delta}]$. Due to the fact that $\delta\mathbf{I} + |\mathbf{V}^\delta|$ is a Hermitian positive-definite matrix, the Cholesky decomposition allows us to decompose it into the product of a lower triangular matrix and its conjugate transpose, i.e.

$$\delta\mathbf{I} + |\mathbf{V}^\delta| = \mathbf{L}\mathbf{L}^*.$$

We want to remark that this decomposition is unique. In addition, $\mathbf{L}$ is invertible, since

$$0 < \det(\delta\mathbf{I} + \mathbf{V}^\delta) = \det(\mathbf{L}) \det(\mathbf{L}^*) = \det(\mathbf{L})\overline{\det(\mathbf{L})}.$$

For each $a > 0$, it follows that

$$\begin{aligned} -a\mathbf{S}_k^\tau + \delta\mathbf{I} + |\mathbf{V}^\delta| &= -a\mathbf{S}_k^\tau + \mathbf{L}\mathbf{L}^* \\ &= \mathbf{L}(-a\mathbf{L}^{-1}\mathbf{S}_k^\tau(\mathbf{L}^*)^{-1} + \mathbf{I})\mathbf{L}^*. \end{aligned}$$

Based on this, we go over to the consideration of the eigenvalues and apply Weyl's Inequality. Since the positive semi-definiteness of $-a\mathbf{S}_k^\tau + \delta\mathbf{I} + |\mathbf{V}^\delta|$ is equivalent to the positive semi-definiteness of $-a\mathbf{L}^{-1}\mathbf{S}_k^\tau(\mathbf{L}^*)^{-1} + \mathbf{I}$, we obtain

$$\theta_j(-a\mathbf{L}^{-1}\mathbf{S}_k^\tau(\mathbf{L}^*)^{-1} + \mathbf{I}) = a\theta_j(-\mathbf{L}^{-1}\mathbf{S}_k^\tau(\mathbf{L}^*)^{-1}) + 1, \quad j = 1, \ldots, M,$$

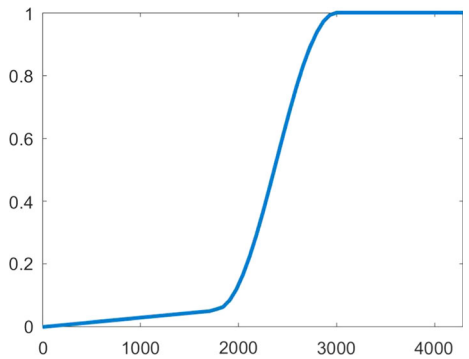

Fig. 11 Transparency function for the plots in Fig. 12 mapping the values of ν to $\alpha(\nu)$

where $\theta_1(A) \geq \cdots \geq \theta_M(A)$ denote the M-eigenvalues of some matrix A.

Further, let $\overline{\theta}_M(-\mathbf{L}^{-1}\mathbf{S}_k^\tau(\mathbf{L}^*)^{-1})$ be the smallest eigenvalue of the matrix $-\mathbf{L}^{-1}\mathbf{S}_k^\tau(\mathbf{L}^*)^{-1}$. Since $\mathbf{S}_k^\tau$ is positive definite, so is $\mathbf{L}^{-1}\mathbf{S}_k^\tau(\mathbf{L}^*)^{-1}$. Thus, $\overline{\theta}_M(-\mathbf{L}^{-1}\mathbf{S}_k^\tau(\mathbf{L}^*)^{-1}) < 0$. Following the lines of [11], we obtain

$$\tilde{\beta}_{k,\delta} = -\frac{1}{\overline{\theta}_M(-\mathbf{L}^{-1}\mathbf{S}_k^\tau(\mathbf{L}^*)^{-1})} \geq 0. \tag{42}$$

4.2.3 Numerical realization

We close this section with a numerical example, where we again consider two inclusions (tumors) in a biological tissue as shown in Fig. 2 (for the values of the Lamé parameter see Table 1). In addition to the Lamé parameters, we use the estimated lower and upper bounds $c^\lambda, c^\mu, C^\lambda, C^\mu$ given in Table 2.

For the implementation, we again consider difference measurements and apply *quadprog* from Matlab in order to solve the minimization problem. In more detail, we perform the following steps:

(1) Calculate

$$\langle(\Lambda(\lambda_0, \mu_0) - \Lambda^\delta(\lambda, \mu))g_i, g_j\rangle_{i,j=1,\cdots,M}$$

with COMSOL to obtain $\mathbf{V}$ via (17).

(2) Evaluate $\hat{\nabla} u^{g_i}_{(\lambda_0,\mu_0)}$ and $\nabla \cdot u^{g_i}_{(\lambda_0,\mu_0)}$ for $i = 1, \cdots, M$, in Gaussian nodes for each tetrahedron.

(3) Calculate $\mathbf{S}^\lambda, \mathbf{S}^\mu$ (cf. Eqs. (14) and (15)) via Gaussian quadrature.
Note that $\mathbf{S}^\lambda, \mathbf{S}^\mu$ can also be calculated from the stiffness matrix of the FEM implementation without additional quadrature errors by the approach given in [10].

(4) Calculate $\mathbf{S}^\tau = \mathbf{S}^\mu + \tau\mathbf{S}^\lambda$ with τ as in (27).

(5) Calculate $\tilde{\beta}_{k,\delta}$, $k = 1, \ldots, p$, as in (42).

(6) Solve the minimization problem (34) with $\mathbf{R}_\delta(v) = \mathbf{S}^\tau v - \mathbf{V}^\delta$ with *quadprog* in Matlab to obtain

$$\tilde{v}_\delta = \sum_{k=1}^{p} a_{k,\delta}\chi_k.$$

(7) Set $\mu = \mu_0 + \tilde{v}_\delta$, $\lambda = \lambda_0 + \tau\tilde{v}_\delta$.

Exact data

We start with exact data, i.e. data without noise and due to the definition of δ given in (18), with $\delta = 0$.

Remark 8 Performing the single implementation steps on a laptop with *2 × 2.5* GHz and 8 GB RAM, we obtained the following computation times: Step (1), i.e., the determination of the matrix $\mathbf{V}$, was done in 9 min 1 s. The Fréchet derivative is computed in 53 s in steps (2)–(4). The solution of the minimization problem (steps (5)–(7)) is calculated in 6 min 27 s.

Figure 12 presents the results as 3D plots, while Fig. 13 shows the corresponding cuts for μ. For the same reasons as discussed in Sect. 3, we change the transparency of the plots of the 3D reconstruction of Fig. 12 as indicated in Fig. 11. Thus, tetrahedrons with low values have a higher transparency, whereas tetrahedrons with large values are plotted opaque.

Figures 12 and 13 show that solving the minimization problem (37) indeed yields a detection and reconstruction with respect to both Lamé parameters μ and λ.

Remark 9 Compared with the results obtained with the one-step linearization method as depicted in Fig. 4 (right hand side), Fig. 12 shows an improvement because we are now able to also obtain information concerning λ which is not possible with the heuristic approach considered in (16).

Noisy data

Finally, we take a look at noisy data with a relative noise level $\eta = 10\%$, where the δ is determined as given in (18).

Figures 14 and 15 document that we can even reconstruct the inclusions for noisy data which is a huge advantage compared with the results of the one-step linearization (see Fig. 8- 9). This shows us, that the numerical simulations based on the monotonicity-based regularization are only marginally affected by noise as we have proven in theory, e.g., in Theorem 2.

5 Summary

In this paper we introduced a standard one-step linearization method applied to the Neumann-to-Dirichlet operator as a heuristical approach and a monotonicity-based regularization for solving the resulting minimization problem. In addition, we proved the existence of such a minimizer. Finally, we presented numerical examples.

Funding Open Access funding enabled and organized by Projekt DEAL.

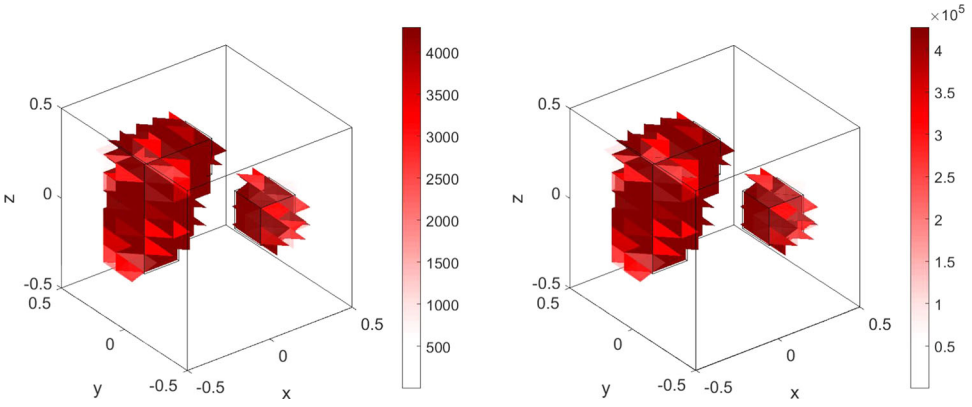

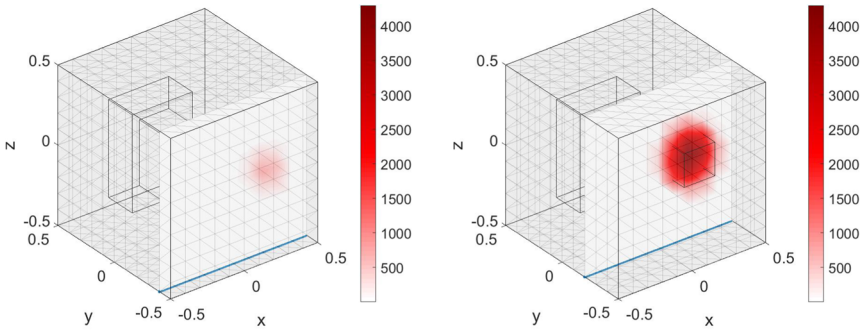

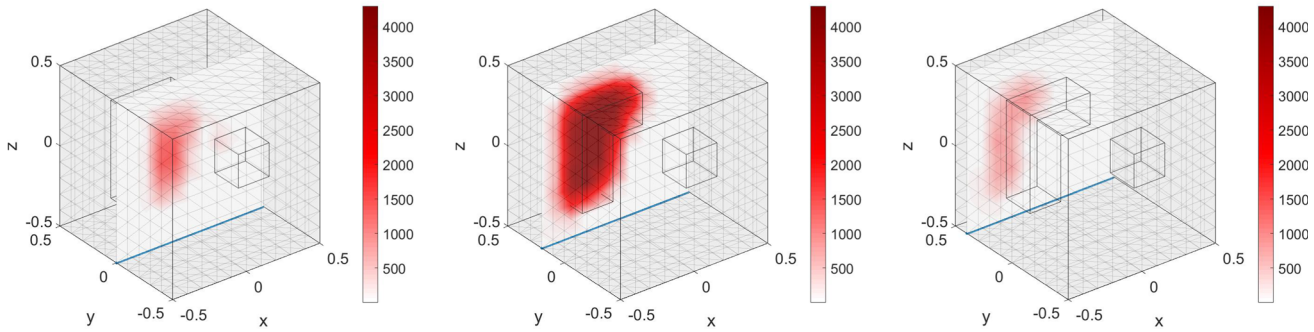

Fig. 12 Shape reconstruction of two inclusions (red) of the reconstructed difference in the Lamé parameter μ (left hand side) and λ (right hand side) without noise, $\delta = 0$ and transparency function α as shown in Fig. 11. (Color figure online)

Fig. 13 Shape reconstruction of two inclusions (red) of the reconstructed difference in the Lamé parameter μ depicted as cuts without noise and $\delta = 0$. (Color figure online)

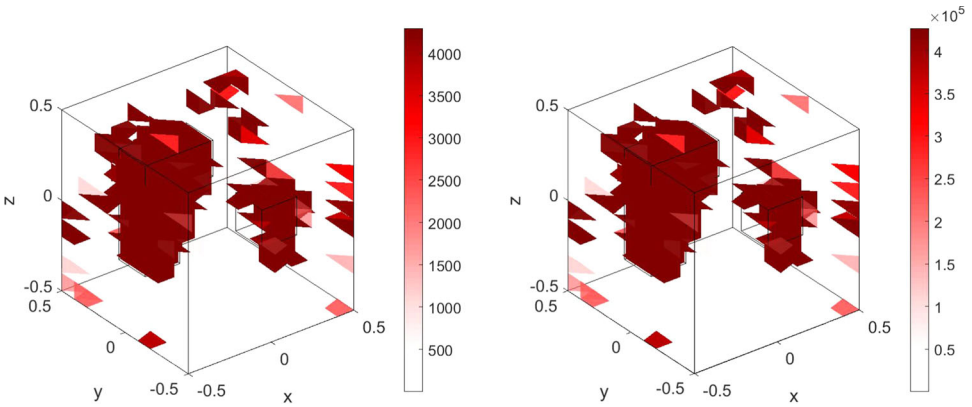

Fig. 14 Shape reconstruction of two inclusions (red) of the reconstructed difference in the Lamé parameter μ (left hand side) and λ (right hand side) with relative noise $\eta = 10\%$, $\delta = 8.3944 \cdot 10^{-8}$ and transparency function α as shown in Fig. 11. (Color figure online)

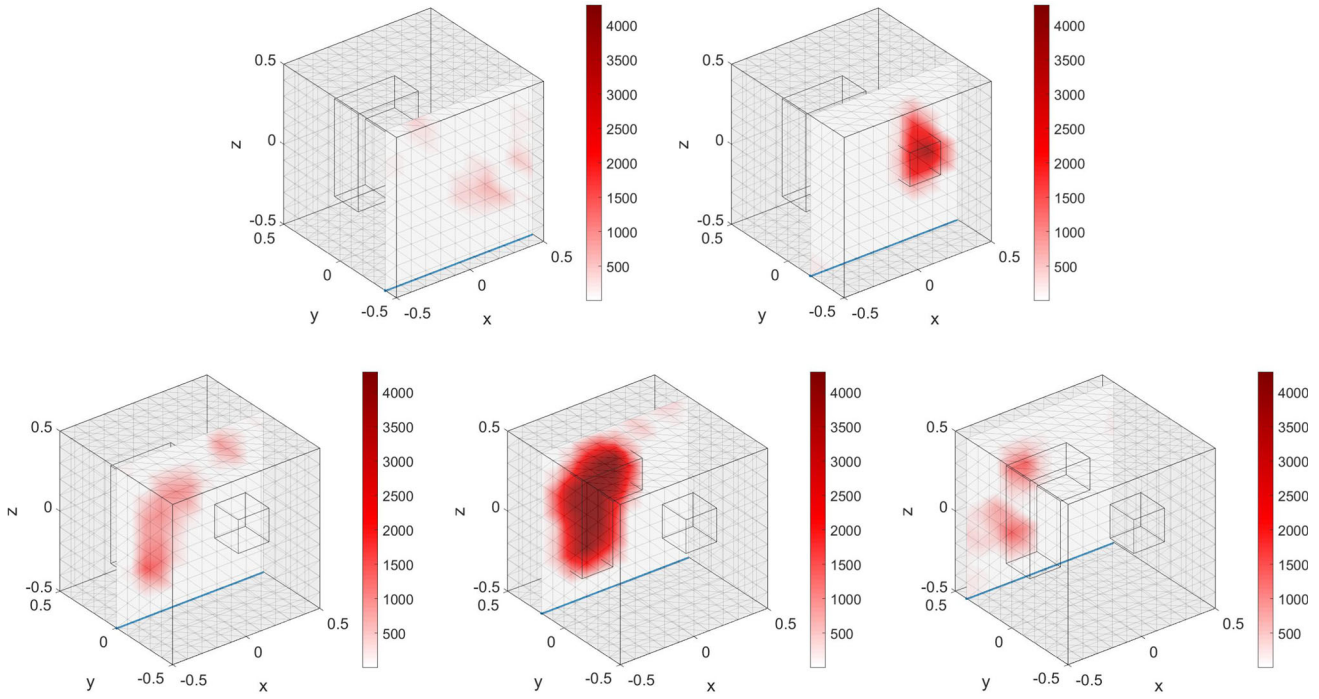

Fig. 15 Shape reconstruction of two inclusions (red) of the reconstructed difference in the Lamé parameter μ depicted as cuts with relative noise $\eta = 10\%$ and $\delta = 8.3944 \cdot 10^{-8}$. (Color figure online)

Appendix

For the monotonicity-based regularization we focused on the case $\lambda \geq \lambda_0, \mu \geq \mu_0$ (see Sect. 5). For sake of completeness, we formulate the corresponding results for the case that $\lambda \leq \lambda_0$, $\mu \leq \mu_0$. Thus, we summarize the corresponding main results and define the set

$$\mathcal{C} := \Big\{ v \in L^\infty(\Omega) : v = \sum_{k=1}^{p} a_k \chi_k,\ a_k \in \mathbb{R},\ 0 \geq a_k \geq -\min(a_{\max}, \beta_k) \Big\}$$

where the quantities $a_{\max}$ and τ are defined as

$$a_{\max} := c^\mu \quad \text{and} \quad \tau := \frac{c^\lambda}{c^\mu}, \tag{43}$$

such that

$$-2(\mu - \mu_0) + 2a \geq 0, \tag{44}$$
$$-(\lambda - \lambda_0) + \tau a \geq 0 \tag{45}$$

for all $0 \geq a \geq -a_{\max}$.

Remark 10 The value $a_{\max}$ is obtained from the estimates in Lemma 1 which results in a different upper bound a compared with the case $\lambda \geq \lambda_0$, $\mu \geq \mu_0$.

Thus, the theorem for exact data is given by

Theorem 3 *Consider the minimization problem*

$$\min_{v \in \mathcal{C}} \|\mathbf{R}(v)\|_F. \tag{46}$$

The following statements hold true:

(i) Problem (46) admits a unique minimizer $\hat{v}$.
(ii) $\operatorname{supp}(\hat{v})$ *and* $\mathcal{D}$ *agree up to the pixel partition, i.e. for any pixel* $\mathcal{B}_k$

$$\mathcal{B}_k \subset \operatorname{supp}(\hat{v}) \quad \textit{if and only if} \quad \mathcal{B}_k \subset \mathcal{D}.$$

Moreover,

$$\hat{v} = \sum_{\mathcal{B}_k \subseteq \mathcal{D}} -a_{\max} \chi_k.$$

The corresponding results for noisy data is formulated in the following theorem, where $\mathbf{R}_\delta(v)$ represents the matrix $(\langle g_i, r_\delta(v) g_j \rangle)_{i,j=1,\dots,M}$ and the admissible set for noisy data

is defined by

$$\mathcal{C}_\delta := \Big\{ \nu \in L^\infty(\Omega) : \nu = \sum_{k=1}^{p} a_k \chi_k,\ a_k \in \mathbb{R},\ 0 \geq a_k \geq -\min(a_{\max}, \beta_{k,\delta}) \Big\}.$$

Theorem 4 *Consider the minimization problem*

$$\min_{\nu \in \mathcal{C}_\delta} \|\mathbf{R}_\delta(\nu)\|_F. \tag{47}$$

The following statements hold true:

(i) Problem (47) admits a minimizer.

(ii) Let $\hat{\nu} = \sum_{\mathcal{B}_k \subseteq \mathcal{D}} -a_{\max}\chi_k$ *be the minimizer of (46) and* $\hat{\nu}_\delta = \sum_{k=1}^{p} a_{k,\delta}\chi_k$ *of problem (47), respectively. Then* $\hat{\nu}_\delta$ *converges pointwise and uniformly to* $\hat{\nu}$ *as* δ *goes to* 0.

References

1. Andrieux S, Abda AB, Bui HD (1999) Reciprocity principle and crack identification. Inverse Probl 15:59–65
2. Beretta E, Francini E, Morassi A, Rosset E, Vessella S (2014) Lipschitz continuous dependence of piecewise constant Lamé coefficients from boundary data: the case of non-flat interfaces. Inverse Probl 30(12):125005
3. Beretta E, Francini E, Vessella S (2014) Uniqueness and Lipschitz stability for the identification of Lamé parameters from boundary measurements. Inverse Probl Imaging 8(3):611–644
4. Ciarlet PG (1978) The finite element method for elliptic problems. North Holland Publishing Co., Amsterdam
5. Eberle S, Harrach B (2021) Shape reconstruction in linear elasticity: standard and linearized monotonicity method. Inverse Probl 37(4):045006
6. Eberle S, Harrach B, Meftahi H, Rezgui T (2021) Lipschitz stability estimate and reconstruction of Lamé parameters in linear elasticity. Inverse Probl Sci Eng 29(3):396–417
7. Eberle S, Moll J (2021) Experimental detection and shape reconstruction of inclusions in elastic bodies via a monotonicity method. Int J Solids Struct. 233:111169
8. Eskin G, Ralston J (2002) On the inverse boundary value problem for linear isotropic elasticity. Inverse Probl 18(3):907
9. Ferrier R, Kadri ML, Gosselet P (2019) Planar crack identification in 3D linear elasticity by the reciprocity gap method. Comput Methods Appl Mech Eng 355:193–215
10. Harrach B (2021) An introduction to finite element methods for inverse coefficient problems in elliptic PDEs. Jahresber Dtsch Math Ver 123:183–210
11. Harrach B, Mach NM (2016) Enhancing residual-based techniques with shape reconstruction features in electrical impedance tomography. Inverse Probl 32(12):125002
12. Harrach B, Ullrich M (2013) Monotonicity-based shape reconstruction in electrical impedance tomography. SIAM J Math Anal 45(6):3382–3403
13. Hubmer S, Sherina E, Neubauer A, Scherzer O (2018) Lamé parameter estimation from static displacement field measurements in the framework of nonlinear inverse problems. SIAM J Imaging Sci 11(2):1268–1293
14. Ikehata M (1990) Inversion formulas for the linearized problem for an inverse boundary value problem in elastic prospection. SIAM J Appl Math 50(6):1635–1644
15. Imanuvilov OY, Yamamoto M (2011) On reconstruction of Lamé coefficients from partial Cauchy data. J Inverse Ill-Posed Probl 19(6):881–891
16. Jadamba B, Khan AA, Raciti F (2008) On the inverse problem of identifying Lamé coefficients inlinear elasticity. Comput Math Appl 56:431–443
17. Lin YH, Nakamura G (2017) Boundary determination of the Lamé moduli for the isotropic elasticity system. Inverse Probl 33(12):125004
18. Marin L, Lesnic D (2002) Regularized boundary element solution for an inverse boundary value problem in linear elasticity. Commun Numer Methods Eng 18:817–825
19. Marin L, Lesnic D (2005) Boundary element-Landweber method for the Cauchy problem in linear elasticity. IMA J Appl Math 70(2):323–340
20. Nakamura G, Tanuma K, Uhlmann G (1999) Layer stripping for a transversely isotropic elastic medium. SIAM J Appl Math 59(5):1879–1891
21. Nakamura G, Uhlmann G (1993) Identification of Lamé parameters by boundary measurements. Am J Math 115:1161–1187
22. Nakamura G, Uhlmann G (1995) Inverse problems at the boundary for an elastic medium. SIAM J Math Anal 26(2):263–279
23. Nakamura G, Uhlmann G (2003) Global uniqueness for an inverse boundary value problem arising in elasticity. Invent Math 152(1):205–207
24. Oberai AA, Gokhale NH, Doyley MM, Bamber JC (2004) Evaluation of the adjoint equation based algorithm for elasticity imaging. Phys Med Biol 49(13):2955–2974
25. Oberai AA, Gokhale NH, Feijoo GR (2003) Solution of inverse problems in elasticity imaging using the adjoint method. Inverse Probl 19:297–313
26. Seidl DT, Oberai AA, Barbone PE (2019) The coupled adjoint-state equation in forward and inverse linear elasticity: incompressible plane stress. Comput Methods Appl Mech Eng 357:112588
27. Steinhorst P, Sändig AM (2012) Reciprocity principle for the detection of planar cracks in anisotropic elastic material. Inverse Probl 29:085010
28. Tamburrino A (2006) Monotonicity based imaging methods for elliptic and parabolic inverse problems. J Inverse Ill-Posed Probl 14(6):633–642
29. Tamburrino A, Rubinacci G (2002) A new non-iterative inversion method for electrical resistance tomography. Inverse Probl 18(6):1809